Pure Appl. Geophys. 171 (2014), 913–940

DOI 10.1007/s00024-013-0685-7

Pure and Applied Geophysics

# Land Surface Temperature Patterns in the Urban Agglomeration of Krakow (Poland) Derived from Landsat-7/ETM+ Data

Jakub P. Walawender,[1,2] Mariusz Szymanowski,[3] Monika J. Hajto,[4] and Anita Bokwa[2]

*Abstract*—The aim of this study was to identify typical and specific features of land surface temperature (LST) distribution in the city of Krakow and its surroundings with the use of Landsat/ETM+ data. The paper contains a detailed description of the study area and technical properties of the Landsat program and data, as well as a complete methodology of LST retrieval. Retrieved LST records have been standardized in order to ensure comparability between satellite images acquired during different seasons. The method also enables identification of characteristic thermal regions, i.e. areas always colder and always warmer than a zonal mean LST value for Krakow. The research includes spatial analysis of the standardized LST with regard to different land cover types. Basic zonal statistics such as mean standardized LST and percentage share of hot and cold regions within 10 land cover types were calculated. GIS was used for automated data processing and mapping. The results confirmed the most obvious dependence of the LST on different land cover types. Some more factors influencing the LST were recognized on the basis of detailed investigation of the LST pattern in the urban agglomeration of Krakow. The factors are: emission of anthropogenic heat, insolation of the surfaces depending first of all on land relief and shape of buildings, seasonal changes of vegetation and weather conditions at the time of satellite image acquisition.

**Key words:** Landsat, ETM+, land surface temperature, single-channel algorithm, thermal regions, Krakow.

## 1. Introduction

Anthropogenic transformations of the natural environment are especially visible in urban areas. One of the most important and broadly studied effects of urban climate is air temperature increase in the city in contrast to the surrounding areas, triggered among other factors by the emission of anthropogenic heat and the higher heat capacity of urban surfaces. This is the so-called urban heat island (UHI) effect, which is a very significant, man-made, but inadvertent local climate modification (Oke 1987). Apart from atmospheric UHI, defined with the use of stationary and mobile air temperature measurements, surface UHI is distinguished due to the differences in surface temperature, usually obtained via remote sensing. Modification of air and surface temperature fields significantly alters living standards for populations around the world. It causes overheating of urban areas, especially in summer, but it may also have positive consequences, e.g. reducing energy use in cold climates during winter. The UHI effect continues to grow with ongoing, rapid urbanization. By 2050, about 70 % of the global population will most likely live in cities (UN-HABITAT Report 2010, 2012).

Significant progress has been made in satellite remote sensing technology in recent years, as well as in continuously improving accessibility to satellite data, resulting in increasing application of this source of information for the monitoring of different processes occurring on the Earth's surface and in the atmosphere. Satellite remote sensing plays an important role in detecting environmental changes, including man-made transformations of the natural environment. Moreover, as opposed to traditional measurement and observation methods executed at specific locations, satellite data are a source of spatially continuous information, which is a huge advantage of this technology. Remotely-sensed images are especially useful for the investigation of

[1] Satellite Remote Sensing Centre, Institute of Meteorology and Water Management–National Research Institute, 14 Borowego St., Krakow, Poland. E-mail: jakub.walawender@imgw.pl
[2] Institute of Geography and Spatial Management, Jagiellonian University, 7 Gronostajowa St., Krakow, Poland.
[3] Institute of Geography and Regional Development, University of Wroclaw, 1 Uniwersytecki Sq., Wroclaw, Poland.
[4] Department of Air Pollution Monitoring and Modelling, Institute of Meteorology and Water Management, National Research Institute, 14 Borowego St., Krakow, Poland.

surface thermal conditions in urban areas. Land surface temperature (LST), the key variable describing thermal conditions, can be retrieved from satellite records. Various research activities on LST distribution based on satellite data were carried out for many cities all over the world: North American cities like Los Angeles, California (Carlson *et al.* 1977; Roth *et al.* 1989), New York City (Price 1979), St. Louis, Missouri (Vukovich 1983), Seattle, Washington and Vancouver, British Columbia (Roth *et al.* 1989), Phoenix, Arizona (Lougeay *et al*. 1996), Huntsville, Alabama (Lo *et al*. 1997), and Houston, Texas (Streutker 2002); Asian cities like Singapore (Nichol 1996), Zhujiang Delta urban areas (Weng 2001), Shanghai (Tran *et al*. 2006; Li *et al*. 2009), Tokyo, Seoul, Beijing, Pyongyang, Bangkok, Manila and Ho Chi Minh City (Tran *et al*. 2006); as well as European cities like Athens (Stathopoulou and Cartalis 2009), Belgrade, Bucharest, Budapest, Milan, Munich, Sofia, Vienna, Warsaw, and Zagreb (Pongrácz *et al*. 2010). A review of thermal remote sensing applications in urban climate studies has been performed by Voogt and Oke (2003), Weng (2009) and Tomlinson *et al*. (2011).

Anthropogenic modifications of surface and air temperature have been also studied in the city of Krakow, in southern Poland, since 1970s. The methods used are comprised of stationary network measurements (e.g. Lewińska and Zgud 1980; Bokwa 2010), thermal aerial photographs from airplane traverses (e.g. Lewińska *et al*. 1990), mobile measurements (e.g. Bokwa *et al*. 2008; Bokwa 2010), measurements aimed to study the vertical thermal structure of the urban boundary layer using sonar (e.g. Walczewski and Feleksy-Bielak 1988), airborne meteorography observations (e.g. Morawska-Horawska and Cebulak 1981), and tethered balloon measurements (e.g. Lewińska and Zgud 1980). However, for the research activities mentioned above, no satellite data were used and moreover, the results obtained cannot be used today for modern spatial analyses due to the methods applied.

First attempts to employ satellite data to study LST distribution in Krakow were made by Struzik (1998) and continued by Hajto (2009). These studies employed NOAA/AVHRR data with the sub-satellite spatial resolution of approximately 1 km. Walawender and Hajto (2009) reviewed and evaluated different algorithms of LST retrieval from images obtained by four different operational satellite radiometers (Meteosat/SEVIRI, NOAA/AVHRR, Terra/MODIS and Landsat/TM) and made a comparative analysis of the created LST maps for the agglomeration of Krakow. The study revealed a great potential of Landsat data for urban-scale evaluation of thermal contrast between different surface types in comparison to meteorological satellites, mainly due to the relatively high spatial resolution. The research has been continued in order to find out details on spatial distribution of LST in Krakow and its surroundings based on Landsat data (Walawender 2009). Only two multispectral Landsat TM and ETM+ images were used. Significant thermal contrasts between different natural and anthropogenic land cover types were identified. The warmest and the coldest objects were indicated. In this study, however, only two cases were taken into account and the images were processed and investigated separately which is an evident shortcoming.

The purpose of this study was to employ Landsat/ETM+ data and GIS techniques in order to evaluate the spatial distribution of the LST in the agglomeration of Krakow, in relation to different natural and anthropogenic factors. The authors propose standardization of the LST values to identify thermally characteristic regions (cold and hot spots). The standardization makes it also possible to compare LST values retrieved from images acquired in different atmospheric conditions. Hence, some aspects of seasonal variability of LST over the vegetative period and its dependence on land relief are discussed. The research also takes into consideration weather conditions at the time of satellite image acquisition.

## 2. Study Area

### 2.1. Geographic Location and Topography

The study area is located in southern Poland (Malopolska region) and includes the city of Krakow and its nearest surroundings (Fig. 1a–c). The area is located at the junction of three large geographical

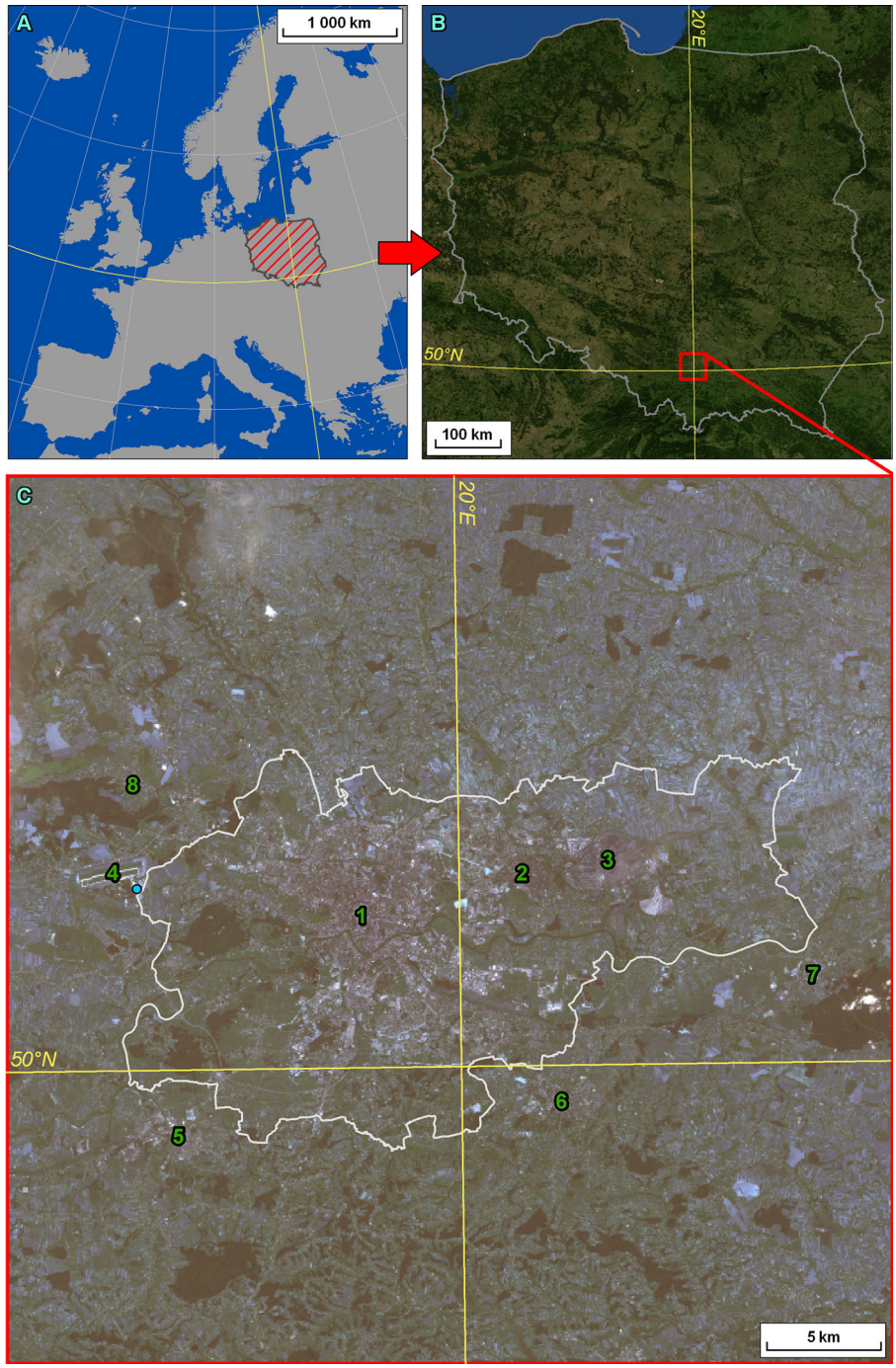


Figure 1

Agglomeration of Krakow: **a** location of Poland in Europe, **b** location of study area in southern Poland (*background layer* NASA's Earth Observatory Blue Marble (2000) for July), **c** study area—agglomeration of Krakow with the nearest surroundings (*background layer* Landsat-7/ETM+ '*True Color*' RGB Composite—July 26, 2000). Characteristic elements of the agglomeration are marked with *green numbers* : *1* Old Town, *2* Center of the Nowa Huta district, *3* steelworks in Nowa Huta, *4* Krakow-Balice International Airport, *5* Skawina town, *6* Wieliczka town, *7* Niepołomice town, *8* Zabierzow village. *Light blue dot* Krakow-Balice weather station. *White line*–Krakow administrative boundary

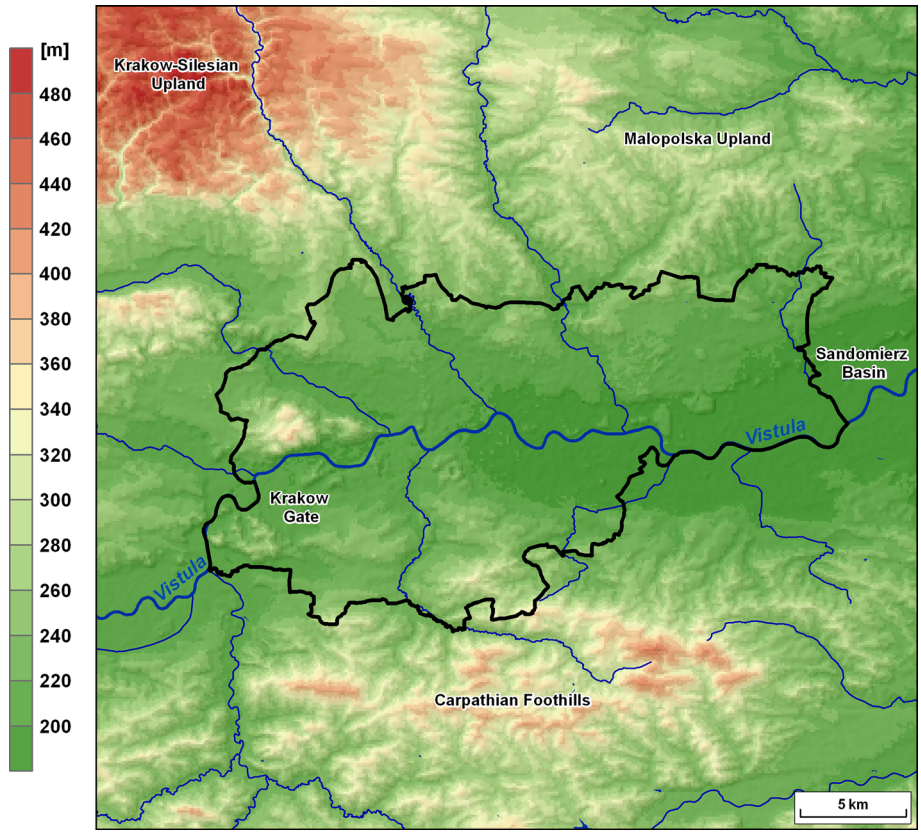


Figure 2
Hypsometry of the study area based on SRTM-3 elevation model resampled to 90 × 90 m resolution. Krakow administrative boundary (*black line*), generalized river network are shown. Main geographic regions are labeled

regions and the relief is quite diversified. The extent of the study area is approximately 1,505 km$^2$ and it was set so that it covered different types of urbanized and natural surfaces that enabled the examination of different factors controlling surface temperature patterns. The city of Krakow is Poland's second largest city and the main economic and cultural center of the Malopolska region. The territory of the city spreads over 326.8 km$^2$ (21.5 % of the whole study area) and the number of registered inhabitants reached 759,137 in 2011 (Demographic Yearbook of Poland 2012). The present shape of Krakow's administrative border (Fig. 1c) and inner urban structure are strictly linked to the history of the city. Concentric development of the city progressed until the mid-20th century, interrupted when a huge steelworks and a new residential area called Nowa Huta were built approximately 12 km to the east of the Krakow's city center. As a result, the city has grown eastwards.

The relief of the study area is diversified (Fig. 2). The city of Krakow is located in the Vistula (Wisla) River valley. Only the southernmost districts of Krakow are located in the Carpathian Foothills, and the northernmost parts of the city belong to the Krakow–Silesian Upland and the Malopolska Upland. The Krakow–Silesian Upland in the northwestern part of the study area represents a typical Jurassic landscape: limestone rocks and deep river valleys covered with mixed forests. On the other hand, the northeastern part of the study area, which is the Proszowice Plateau (a part of the Malopolska Upland) with very fertile soils, is almost completely deforested and used mainly for agriculture. There are a few isolated tectonic horsts in the western part of the study area called the Krakow Gate (Brama Krakowska). Some of these horsts are located within the administrative limits of Krakow. The Vistula River valley is very narrow there (up to 1 km) as

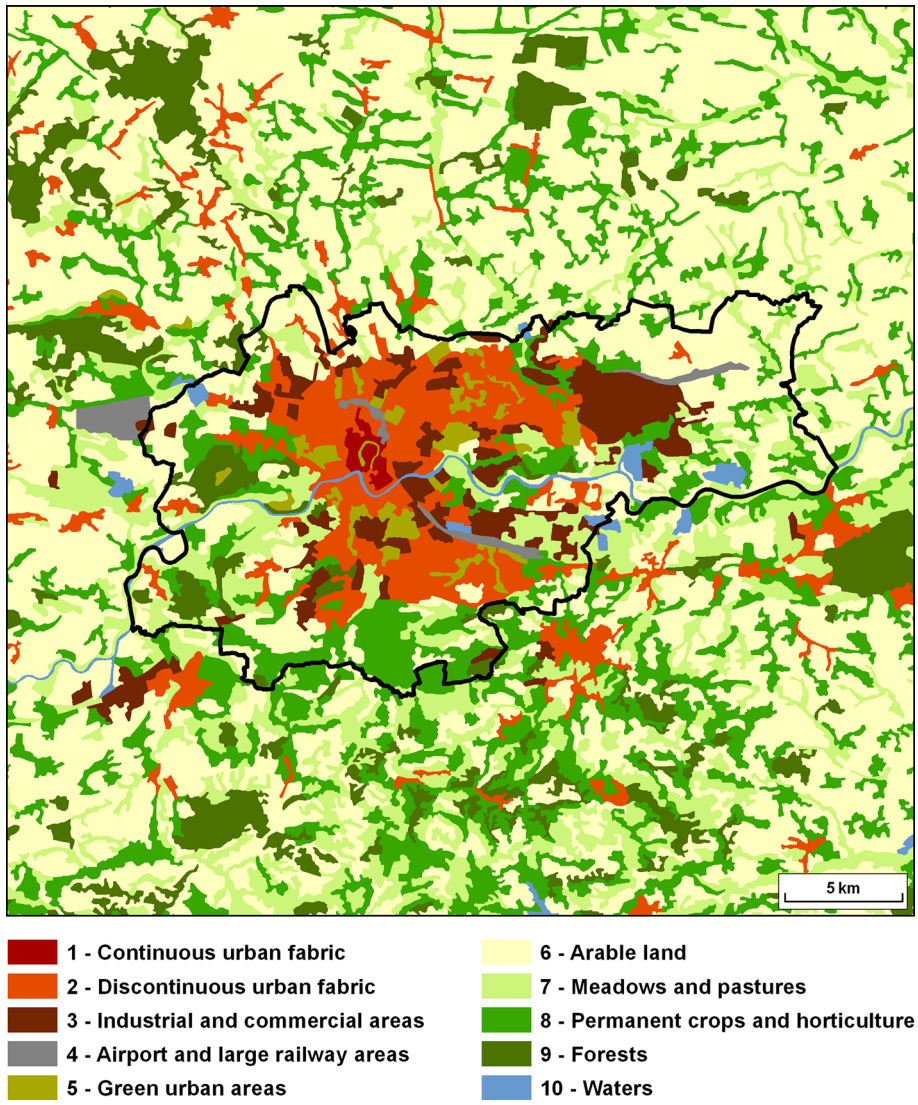


Figure 3
Land cover structure of the study area based on generalized CORINE Land Cover 2000 database

opposed to the eastern part of the study area where it widens up to 10 km. The eastern part of the study area belongs to the Sandomierz Basin. The Carpathian Foothills, i.e. the outermost part of the Polish Western Carpathians, are located in the southern part of the study area, formed by low hills with oval slopes.

The elevation difference between the highest and the lowest point within the study area reaches up to 300 m and the difference between the Vistula River valley bottom and the tops of the nearby convex land forms is on average about 100 m.

### 2.2. *Land Cover Structure*

Krakow and its nearest surroundings are highly diversified in terms of land cover (Fig. 3). Land cover structure by percentage share was calculated on the basis of CORINE Land Cover database (see Sect. 3.2 for details) separately for the whole study area and for the city of Krakow (Fig. 4). Most of the land within the study area is used for agricultural purposes (arable land, orchards, meadows)—nearly 80 %, while urban fabric, industrial, commercial and transportation facilities comprise only about 11 % of the

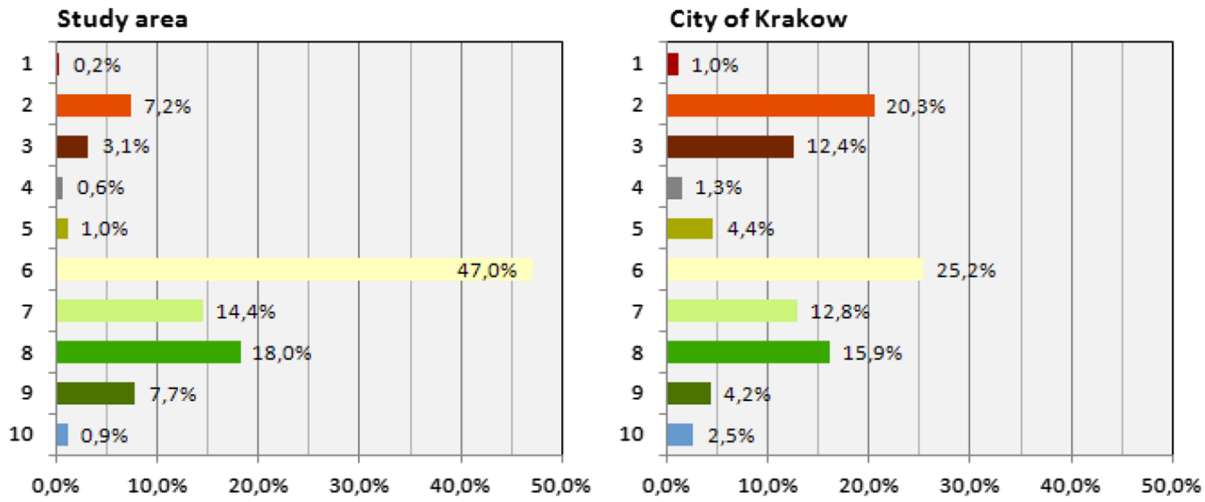


Figure 4
Land cover structure within the study area (*left*) and in the Krakow city limits (*right*) by percentage share [description of land cover types (*1–10*) in Fig. 3]

total area. The rest is made up of forests and artificial vegetated area (about 8 %), and also water bodies (about 1 %). The proportion changes when taking into account only the territory of Krakow: the percentage of artificial surfaces raises up to 35 % while the percentage of arable lands, orchards, and meadows falls down to about 54 %, as there are less forests and more artificial vegetated areas (mainly parks and wooded cemeteries).

The historical center of Krakow is encircled by a "green belt", which is a city park, 4-km long and from 50 to 120-m wide. Further outside from the historical center, some more continuous urban fabric is adjoined. Urban structures and the transport network occupy here more than 80 % of the surface area, and nonlinear areas of vegetation as well as bare soil are exceptional (CORINE Land Cover Technical Guide—Addendum 2000). New housing estates (blocks of flats) are located in the south and in the north of the city. Detached houses are spread randomly among the blocks of flats or are located in the suburbs. There are a few city parks, wooded cemeteries and complexes of allotment gardens. Huge industrial areas are located in the eastern part of the city (steelworks in Nowa Huta) and in Skawina (combined heat and power plant, previously also aluminium plants). Other, smaller industrial objects can be found in different locations all over the city, similar to a few huge shopping malls.

Forests are located mainly in the northwestern part of the study area covering ridges of the Krakow–Silesia Upland and the tectonic horsts, in the broad, eastern part of the Vistula river valley belonging to the Sandomierz Basin and in the Carpathian Foothills in the south. Water reservoirs, which are predominantly artificial (former gravel excavations places or old river beds cut off the Vistula river during hydrological regulation in the 20th century), are located mainly in the vicinity of the city.

## 3. Source Data

### 3.1. Landsat Satellite Program, ETM+ Sensor Characteristics and Selected Imagery

Landsat is the longest running initiative providing multispectral satellite images of the Earth in moderate spatial resolution (15–120 m depending on spectral band), managed jointly by the National Aeronautics and Space Administration (NASA) and the United States Geological Survey (USGS). The history of the Landsat program reaches back to July 26, 1972, when the Earth Resources Technology Satellite (ERTS), later renamed to Landsat-1, was launched. Landsat satellites were primarily designed to supply images of the Earth's surface mostly for detection of land cover changes. Currently, the USGS

Landsat archive constitutes the world's largest collection of moderate resolution satellite data, access to which has remarkably improved after January 2009, when the USGS made all Landsat images freely available (USGS Landsat Website 2012).

Data used in this study were obtained by an Enhanced Thematic Mapper Plus (ETM+) sensor installed aboard Landsat-7. The satellite was successfully launched on April 15, 1999. The satellite's orbit parameters are listed in Table 1. The sun-synchronous orbit achieved by proper regulation of the satellite's altitude and inclination angle keeps Landsat-7 flying over a particular area exactly at the same local mean solar time. This means that illumination of the specified surface is the same every time it is scanned by the satellite. This property is very important for comparison of image sequences used in this study.

A complete 16-day ground coverage cycle for Landsat-7 was divided into 233 scanning paths (indexing successive orbits) and 248 rows (indexing scene centers). The standard, which is called the Worldwide Reference System 2 (WRS-2), makes it easier to find an appropriate Landsat-7/ETM+ scene of specific location in the world. An approximate scene size is 170 km north–south by 183 km east–west.

The ETM+ instrument is a fixed "whisk-broom", moderate resolution, multispectral imaging radiometer operating in the visible (VIS), near-infrared (NIR), short-wave infrared (SWIR), and thermal infrared (TIR) portion of the electromagnetic spectrum. Data are acquired in eight spectral bands (Table 2) with a spatial resolution of 30 m, except for the thermal band (60 m) and the panchromatic band (15 m) (NASA Landsat Project Website 2012).

The main applications of all Landsat/ETM+ spectral bands were summarized by Lillesand and Kiefer (2000). In this study, thermal-infrared band (band 6) data are used to retrieve LST, whereas visible-red band (band 3) and near-infrared band (band 4) are inputs for land surface emissivity calculations. No data after May 2003 were taken into consideration because one of the Landsat/ETM+ subcomponents—scan line corrector (SLC) failed permanently, disabling the ability of the sensor to maintain a rectilinear scanning pattern.

Table 1

*Landsat-7 orbit parameters (Irish 2003)*

| | |
|---|---|
| Regime | Circular, repetitive, near-polar, sun-synchronous |
| Inclination | 98.2° |
| Altitude | 705.3 km (±5 km) |
| Equatorial crossing time | 10:00 am (±15 min) local time (descending node) |
| Orbital period | 98.8 min (~14.5 orbits/day) |
| Revisit time | 16 days (233 orbits) |

Table 2

*ETM+ spectral bands*

| Band number | Spectral range | |
|---|---|---|
| | Nominal | Wavelength (μm) |
| 1 | Visible-blue | 0.45–0.52 |
| 2 | Visible-green | 0.52–0.60 |
| 3 | Visible-red | 0.63–0.69 |
| 4 | Near-infrared | 0.76–0.90 |
| 5 | Shortwave-infrared | 1.55–1.75 |
| 6 | Thermal-infrared | 10.4–12.5 |
| 7 | Shortwave-infrared | 2.08–2.35 |
| 8 | Panchromatic | 0.50–0.90 |

The source of the Landsat/ETM+ image collection was the USGS Landsat data archive, accessed via special online search and order tools: USGS Global Visualisation Viewer (GLOVIS) available at: http://glovis.usgs.gov and EarthExplorer (http://earthexplorer.usgs.gov/). The processing level of the downloaded data was 1T, which means the images were radiometrically and geometrically corrected. Only six fully valuable Landsat-7/ETM+ images acquired in different months of the vegetative period were chosen (Table 3) out of all 37 Landsat-7/ETM+ SLC on scenes covering agglomeration of Krakow (WRS-2 coordinates: path 188, row 25) that existed in the USGS Archive. The number of selected images was limited because of strict selection conditions established to ensure high quality of the results. As the main objective was the delimitation of thermal regions in Krakow area, only the images with no clouds, fog and a minimum of smoke within the administrative border of the city were taken into account.

The selected images represent six different stages of the vegetative period (from early March to mid-August) with different plant cover and weather

conditions before and at the time of the satellite data acquisition. Weather conditions at the time of satellite images acquisition were analyzed on the basis of measurements and observations made at the weather station Krakow-Balice (latitude, 50°48′07″N; longitude, 19°48′07″E; height, 237 m a.s.l.; Fig. 1c—blue dot). It is the only station in the Krakow area with meteorological measurements and observations provided every hour. The meteorological records were also used for atmospheric correction during LST retrieval. The atmospheric parameters are listed in Table 4. Near-real conditions at the time of images acquisition were simulated by calculating mean air temperature and mean relative humidity of observations made at 9:00 and 10:00 UTC.

Table 3

*Basic characteristics of the Landsat-7/ETM+ scenes used in the study*

| Date | Scene center scan time (UTC) | Sun azimuth (°) | Sun elevation (°) | Cloud cover (%) |
|---|---|---|---|---|
| Mar 7, 2001 | 9:22:47 | 153.9 | 31.3 | 0 |
| Apr 21, 2000 | 9:24:44 | 151.7 | 48.8 | 3 |
| May 7, 2000 | 9:24:38 | 149.9 | 53.6 | 1 |
| May 26, 2001 | 9:22:16 | 146.1 | 57.3 | 1 |
| Jul 26, 2000 | 9:23:39 | 144.3 | 54.9 | 16 |
| Aug 17, 2002 | 9:20:37 | 147.5 | 49.3 | 12 |

### 3.2. Auxiliary Datasets

Apart from the Landsat-7/ETM+ data, multiple other digital geo-datasets were used in the study, including:

- CORINE Land Cover 2000 (CLC2000) PL—vector database containing land cover data of Poland observed between 1999 and 2001. EU CORINE Land Cover data fulfill thematic and geometric standards. The scale of datasets is 1:100,000 and the smallest mapping unit is 25 ha

Table 4

*Weather conditions at the time of images acquisition. Air temperature and relative humidity at the time of image acquisition were estimated as the mean value of the observations done at 9:00 and 10:00 UTC*

| Atmospheric parameter | Date of landsat image acquisition | | | | | |
|---|---|---|---|---|---|---|
| | Mar 7, 2001 | Apr 21, 2000 | May 7, 2000 | May 26, 2001 | July 26, 2000 | Aug 17, 2002 |
| Air temperature (°C) | | | | | | |
| 9:00 UTC | 2.5 | 19.3 | 19.6 | 14.0 | 24.3 | 20.3 |
| 10:00 UTC | 5.3 | 21.9 | 21.1 | 14.6 | 25.3 | 22.2 |
| Mean | 3.9 | 20.6 | 20.4 | 14.3 | 24.8 | 21.3 |
| Relative humidity (%) | | | | | | |
| 9:00 UTC | 68 | 72 | 49 | 45 | 52 | 80 |
| 10:00 UTC | 55 | 53 | 38 | 38 | 49 | 69 |
| Mean | 62 | 63 | 44 | 32 | 51 | 75 |
| Visibility (km) | | | | | | |
| 9:00 UTC | 6 | 8 | 30 | 50 | 30 | 8 |
| 10:00 UTC | 10 | 20 | 30 | 50 | 50 | 10 |
| Cloud cover (%) | | | | | | |
| 9:00 UTC | 0 | 12 | 0 | 62 | 12 | 12 |
| 10:00 UTC | 0 | 12 | 0 | 88 | 25 | 12 |
| Wind direction: | | | | | | |
| 9:00 UTC | E | SW | NE | NE | NE | SW |
| 10:00 UTC | Variable | S | E | Variable | Variable | – |
| Wind speed (m/s) | | | | | | |
| 9:00 UTC | 1 | 1 | 5 | 2 | 1 | 1 |
| 10:00 UTC | 2 | 1 | 5 | 2 | 2 | 0 |
| Atmospheric phenomena | | | | | | |
| Current | Mist | Mist, Cu clouds | Clear sky | Ci clouds | Cu and Ci clouds | Mist, Cu and Ac clouds |
| Past | Clear sky | Fog | Clear sky | Increasing cloudiness | Increasing cloudiness | Fog |

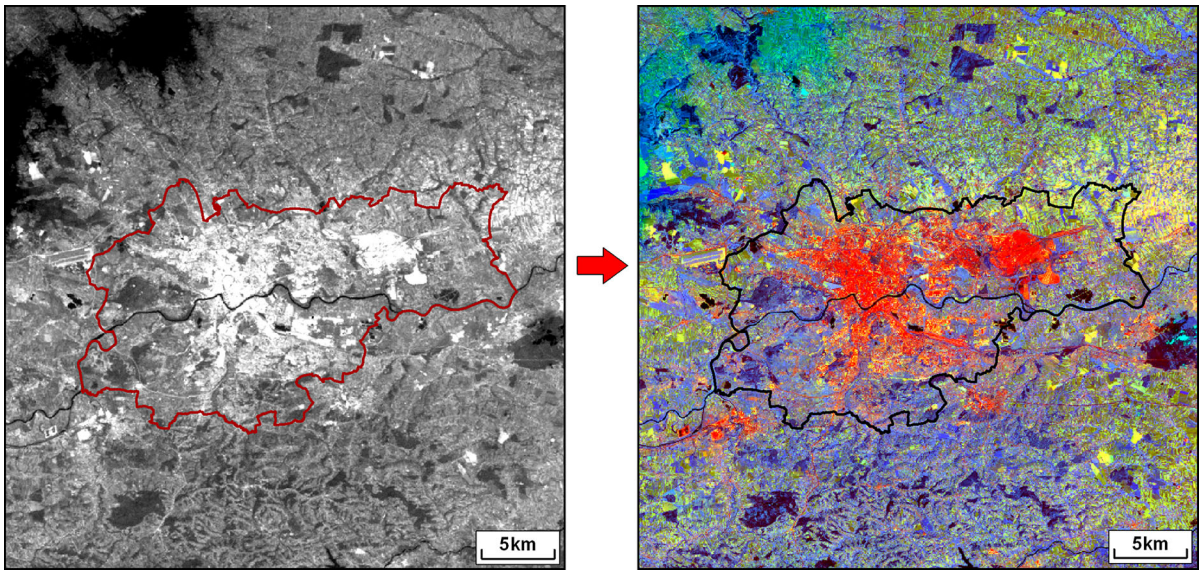


Figure 5
ETM+ band 6 (thermal) 8-bit *greyscale* image of the study area (*left*) and image composite of three infrared bands of the ETM+ radiometer RGB = 654 (*right*) (acquisition date July 26, 2000)

(Bielecka and Cioikosz 2004). Source of data: EEA Data and Maps (2012).

- GMES European Urban Atlas PL003L v.1.1—vector database providing pan-European comparable land use and land cover data for Large Urban Zones with more than 100,000 inhabitants. Code PL003L means agglomeration of Krakow. Minimum mapping unit is 0.25–1 ha (GMES—Mapping Guide for a European Urban Atlas v. 1.01 2010).
- SRTM Digital Elevation Model v4.1—hole-filled, seamless near-global coverage gridded elevation data processed by the International Centre for Tropical Agriculture (CIAT) from original USGS/NASA SRTM-3 data. They are provided in mosaiced 5° × 5° tiles with spatial resolution of 3 arc seconds, which is approx. 90 × 90 m (Jarvis *et al.* 2008).
- High-resolution color orthophotomaps—a set of 21 georeferenced aerial photographs with spatial resolution of 0.25 m (image scale 1:5,000) covering selected regions of special interest within the study area. The photographs were acquired on 25 and 28 July 2009 (Geoportal 2012).

There were two reasons for employing vector CORINE Land Cover Dataset in order to estimate the land cover structure in the agglomeration of Krakow. First of all, Landsat ETM+ images acquired between 1999 and 2001 were primarily used to develop the CLC2000 (Bielecka and Cioikosz 2004). Secondly, the CLC2000 was used and validated many times during numerous research activities (Stathopoulou *et al.* 2004; Stathopoulou and Cartalis 2007; Yilmaz 2010; Petrişor *et al.* 2010; Maucha and Büttne 2006), and is an accepted source of information about land cover among many professionals. Initially, the generalized CLC2000 layer was further used in the study to calculate the minimum, maximum and mean LST for ten land cover types.

## 4. Methods and Tools

The Landsat ETM+ radiometer measures energy ranging from the visible part of the electromagnetic spectrum to the far infrared. The visible wavelengths are solar energy, which is reflected from the objects on the Earth's surface or clouds and aerosols that can be found in the atmosphere, whereas far infrared wavelengths are emitted terrestrial energy (Schowengerdt 2007) as a function of the object's temperature and its emission capacities.

A sample 8-bit thermal image showing the study area in shades of grey is presented below (Fig. 5, left). In this image, darker pixels refer to colder objects and brighter pixels to warmer objects. The grey-scale image, however, is difficult to read by the human eye. An image that is much easier to interpret can be obtained by mixing spectral responses of three infrared bands in one RGB composite (Red, band 6; Green, band 5; Blue, band 4). This visualization technique can be applied to combine images with different pixel sizes. The infrared RGB composite (Fig. 5, right) depicts the warmest objects in red and the coldest in very dark grey, blue and violet, which is a much more intuitive color scale for the surface temperature interpretation. This color composite has to be, however, carefully interpreted as it gives the possibility of observing land below cirrus clouds, which are visible in the northwest corner of the thermal band image presented below (Fig. 5). The cirrus clouds are present in the composite image (turquoise-green colors) but are not easy to see due to the visible component of the short infrared red bands that penetrates partly through the thin clouds. Interpretations of thermal characteristics of the surface below cirrus clouds are very risky as the radiation registered by the satellite sensor comes not only from the Earth's surface but also from the clouds.

Both the grey-scale image and the color composite provide only qualitative information about thermal patterns of the surface. It means that colder and warmer objects can be identified but no particular temperature values for each pixel. Therefore, for more detailed research, the digital number of the Landsat ETM+ thermal image has to be converted to the LST.

### 4.1. Land Surface Temperature (LST) Retrieval

The procedure used in this study in order to derive LST from the selected Landsat/ETM+ data includes the following steps:

Conversion of pixel values of the Landsat thermal data in level 1 product generation system (LPGS) format to at-sensor spectral radiance ($L_s$) in W m$^{-2}$ sr$^{-1}$ μm$^{-1}$ according to the following equation:

$$L_s = \text{gain} \cdot \text{DN} + \text{bias}, \tag{1}$$

where DN is a digital number (the pixel value); and gain (the slope of the radiance) and bias (the intercept of the radiance) are the DN conversion coefficients—for Landsat-7 ETM+ band 6: gain = 0.037205 and bias = 3.16 (Chander *et al.* 2009).

Application of inverted Planck's Law to transform the at-sensor spectral radiance to at-sensor brightness temperature $T_s$ (Irish 2003):

$$T_s = \frac{K_2}{\ln\left(\frac{K_1}{L_s} + 1\right)} \tag{2}$$

where: $K_1$ and $K_2$ are specific thermal band calibration constants—for Landsat-7 ETM+: $K_1$ = 666.09 W m$^{-2}$ sr$^{-1}$ μm$^{-1}$ and $K_2$ = 1282.71 K (Chander *et al.* 2009).

Conversion of the at-sensor spectral radiance to at-sensor brightness temperature assumes that the earth's surface is a black body with an emissivity value equal to 1 (Li *et al.* 2011).

Estimation of LST values with single-channel (SC) algorithm (Jiménez-Muñoz and Sobrino 2003; Sobrino *et al.* 2004; Jiménez-Muñoz *et al.* 2009; Cristóbal *et al.* 2009):

$$\text{LST} = \gamma\left[\frac{1}{\varepsilon}(\psi_1 L_s + \psi_2) + \psi_3\right] + \delta \tag{3}$$

where $\varepsilon$ is the land surface emissivity (LSE); $\gamma$ and $\delta$ are the Planck's function dependent parameters; and $\psi_1$, $\psi_2$ and $\psi_3$ are the atmospheric functions.

The parameters $\gamma$ and $\delta$ were estimated using the following equations:

$$\gamma = \left\{\frac{c_2 L_s}{T_s^2}\left[\frac{\lambda^4 L_s}{c_1} + \frac{1}{\lambda}\right]\right\}^{-1} \tag{4a}$$

$$\delta = -\gamma \cdot L_s + T_s, \tag{4b}$$

where $c_1$ and $c_2$ are the Planck's radiation constants ($c_1$ = 1.19104 10$^8$ W μm$^4$ m$^{-2}$ sr$^{-1}$; $c_2$ = 1.43877 10$^4$ μm K); and $\lambda$ is the effective wavelength ($\lambda$ = 11.27 μm for Landsat-7/ETM+ band 6).

The SC Algorithm incorporates correction of atmospheric influence and takes into account different emission properties of various land surfaces.

Correction of atmospheric influence requires site-specific atmospheric parameters (atmospheric transmissivity—$\tau$, up-welling atmospheric radiance—$L^{\uparrow}$ and down-welling atmospheric radiance—$L^{\downarrow}$) which are calculated by means of a web-based tool

called an Atmospheric Correction Parameter Calculator (ACPC) (Barsi *et al*. 2003, 2005). The ACPC is available online at http://atmcorr.gsfc.nasa.gov. This tool uses the National Center for Environmental Prediction (NCEP)-modeled atmospheric global profiles, MODTRAN 4.0 radiative transfer codes and the integration algorithms. The ACPC requires a particular date, time and location as input. It is also possible to define local conditions (altitude, pressure, air temperature and relative humidity) that determine interpolation of the modeled atmospheric profile. In this work, data from the weather station at Krakow-Balice were used.

The computed site-specific atmospheric parameters ($\tau$, $L^{\uparrow}$ and $L^{\downarrow}$) were then used to calculate atmospheric functions ($\psi_1$, $\psi_2$ and $\psi_3$) which were necessary input variables for the SC formula (3). The atmospheric functions were defined as follows:

$$\psi_1 = \frac{1}{\tau} \tag{5a}$$

$$\psi_2 = -L^{\downarrow} - \frac{L^{\uparrow}}{\tau} \tag{5b}$$

$$\psi_3 = L^{\downarrow} \tag{5c}$$

Retrieval of land surface emissivity records was performed with the use of normalized difference vegetation index thresholds method ($NDVI^{THM}$) (Sobrino and Raissouni 2000; Sobrino *et al*. 2008). $NDVI^{THM}$ is one of several approaches used to estimate LSE based on normalized difference vegetation index (NDVI) (Van de Griend and Owe 1993; Valor and Caselles 1996). NDVI (Rouse *et al*. 1973; Tucker 1979) is a band ratio defined on the basis of radiation properties of chlorophyll (strongly absorbs visible light for photosynthesis) and cell structure of the leaves (strongly reflects near-infrared radiation). It gives information about green vegetation coverage. For Landsat/ETM+ data, NDVI is calculated as a combination of bands 3 and 4:

$$\mathrm{NDVI} = \frac{\mathrm{Band4} - \mathrm{Band3}}{\mathrm{Band4} + \mathrm{Band3}} \tag{6}$$

The $NDVI^{THM}$ uses certain NDVI values (thresholds) to distinguish between soil pixels ($NDVI < NDVI_S$), pixels of full vegetation ($NDVI > NDVI_V$) and mixed pixels ($NDVI_S \leq NDVI \leq NDVI_V$) considered to be a mixture of soil and vegetation (Sobrino *et al*. 2008).

In this work, the general assumptions of the $NDVI^{THM}$ were simplified. Values of $NDVI_S = 0.2$ and $NDVI_V = 0.5$ proposed bySobrino and Raissouni (2000) for global conditions (applicable over any area in the Earth) were assumed. Using the $NDVI_S$ and $NDVI_V$ values proportion of vegetation ($P_V$), also referred to as fractional vegetation cover—FVC, was derived from NDVI according to Carlson and Ripley (1997):

$$P_V = \left(\frac{\mathrm{NDVI} - \mathrm{NDVI_S}}{\mathrm{NDVI_V} - \mathrm{NDVI_S}}\right)^2 \tag{7}$$

The cavity effect due to surface roughness was corrected using a term $C_\lambda$ , given by:

$$C_\lambda = (1 - \varepsilon_{S\lambda}) \cdot \varepsilon_{V\lambda} \cdot F' \cdot (1 - P_V), \tag{8}$$

where $F'$ is a geometrical factor (ranging between 0 and 1) depending on the geometrical distribution of the surface; in this work, the mean value for rough and heterogonous surface $F' = 0.55$ was chosen according to Sobrino *et al*. (1990). No accurate atmospheric correction is needed when using a scaled NDVI values for estimation of the FVC (Sobrino *et al*. 2008).

Emissivity of soil pixels ($NDVI < NDVI_S$) is set to 0.96 ($P_V = 0$ and $C_\lambda = 0$, so $\varepsilon = \varepsilon_{S\lambda} = 0.96$, where $\varepsilon_{S\lambda}$ is the assumed emissivity of bare soil) and emissivity of full vegetation pixels ($NDVI > NDVI_V$) is set to 0.99 ($P_V = 1$ and $C_\lambda = 0.005$, so $\varepsilon = \varepsilon_{V\lambda} + C_\lambda = 0.985 + 0.005 = 0.99$, where $\varepsilon_{V\lambda}$ is the assumed emissivity of full vegetation). Emissivity of mixed pixels ($NDVI_S \leq NDVI \leq NDVI_V$) was computed according to the formula (Sobrino *et al*. 1990):

$$\varepsilon = \varepsilon_{V\lambda} \cdot P_V + \varepsilon_{S\lambda} \cdot (1 - P_V) + C_\lambda \tag{9}$$

There have been several studies performed on validation and intercomparison of $NDVI^{THM}$ against other methods (Sobrino *et al*. 2008). A comparison between $NDVI^{THM}$ and three other LSE algorithms ($TISI^{BL}$, TS-RAM and Δday) applied to NOAA/AVHRR data over the Iberian Peninsula provided very low values of root mean square error (RMSE) ranging between 0.01 and 0.02 (Sobrino *et al*. 2001). The results achieved after applying $NDVI^{THM}$ to

Landsat/TM data over the Requena-Utiel site (Valencia, Spain) were compared to in situ measurements obtaining the RMSE below 0.01 (Sobrino *et al.* 2004). Application of $NDVI^{THM}$ to AHS imagery of 4-m spatial resolution during the DESIREX 2008 experimental campaign over the city of Madrid (Spain) in comparison with two other LSE methodologies (TES and TISI) showed the lowest RMSE = 0.06 with the use of in situ data from the urban surfaces (Oltra-Carrió *et al.* 2012). Although $NDVI^{THM}$ does not appear to be the best LSE estimation method to be applied for urban studies, it is considered as the most appropriate option for Landsat/TM or ETM+ data (Sobrino *et al.* 2004, 2008; Rodriguez-Galiano *et al.* 2012), even to estimate urban LST pattern (Xiao *et al.* 2007; Mackey *et al.* 2012) because, unlike the other mentioned LSE algorithms, it does not require thermal band or a nighttime image. It should also be noted that the $NDVI^{THM}$ underestimates emissivity values for water bodies (Sobrino *et al.* 2008), as they range between 0.90 and 0.93 and should be close to 1 within visible and thermal infrared wavelengths. This is a serious disadvantage which requires further corrections.

The underestimated LSE values were corrected with a self-developed, three-step procedure:

- Arithmetical division of band 4 (NIR) image by band 3 (VIS red) image in order to classify 'water pixels'.
- Extraction of the depiction result by a water mask created using GMES Urban Atlas PL003L Dataset (removal of pixels wrongly classified as water bodies). GMES Urban Atlas was used to create the water mask instead of CLC Land Cover because of a smaller mapping unit which is 0.25 ha in urban areas and 1 ha in other areas (GMES—Mapping Guide for a European Urban Atlas v. 1.01 2010). Water class includes: lakes, fish ponds (natural, artificial), rivers (incl. channeled rivers) and canals.
- Assignment of a new value of 0.995 for the extracted 'water pixels'. This value was assumed taking into account very low reflectance (up to 1 %) of water bodies in thermal infrared spectral range around the effective wavelength of Landsat/ETM+ band 6 (Salisbury and D'Aria 1992; MODIS UCSB Emissivity Library 2012; ASTER Spectral Library 2012).

The retrieved LSE ($\varepsilon$) output records are one of the necessary inputs for the SC formula (3).

The single-channel method has been approved and commonly applied for thermal conditions research in urban areas by numerous researchers all over the world (Gabor and Jombach 2009; Li *et al.* 2010; Liu and Zhang 2011). In this study, the whole procedure was performed automatically using ESRI ArcGIS Desktop 10.1 with the Spatial Analyst extension and an additional Landsat TRS toolbox created beforehand (Walawender *et al.* 2011, 2012).

### 4.2. *Accuracy Assessment of the SC Algorithm*

The best solution to validate the single-channel algorithm would be to compare the retrieved LST values with in situ ground-truth measurements of the LST (Qin *et al.* 2001). Unfortunately, it is very difficult to obtain ground-truth LST data comparable to the Landsat/ETM + thermal image pixel size of 60 m. The single-channel algorithm has been, however, previously validated for Landsat TM band 6 using ground-truth data by Jiménez-Muñoz and Sobrino (2003) showing root mean square deviations (RMSD) lower than 1.5 K for different land cover types. An alternative approach using simulated data introduced by Sobrino *et al.* (2004) obtained the RMSD of 1.0 K. In this study, the level of LSE influence on LST estimates was evaluated by subtracting all the six output LST maps, estimated with the use of LSE and retrieved with the $NDVI^{THM}$ from a new set of maps, created with exactly the same procedure but applying constant LSE value of 0.97 for each pixel within the whole study area. The value of 0.97 is a rounded mean zonal LSE of all pixels of all six LSE maps derived with $NDVI^{THM}$. Consequently, maximum differences between the LSE values retrieved by modified $NDVI^{THM}$ (masked surface water bodies) and the LSE constant value reached 0.025. The results showed that for the vast majority of pixels (between 96 and 100 % depending on a scene), LST difference is less than 1 K, which is less than single-channel algorithm error estimated by Jiménez-Muñoz and Sobrino (2003) and by Sobrino *et al.* (2004).

### 4.3. Standardization and Geoprocessing of the LST Values

Interpretation of LST distribution in the city of Krakow is not a very easy task because of the combined influence of environmental and anthropogenic factors such as diversified relief, urban land cover mosaic including complex building structures, seasonal changes of vegetation, and variability of atmospheric conditions (weather types). The role of the proposed standardization of the LST values is to enable:

- Objective evaluation of the LST pattern derived from images acquired in different atmospheric conditions and in various phases of the vegetative period.
- Delimitation of more general LST features (thermally characteristic regions).
- Comparative analysis of the LST spatial variability in relationship to different land cover types for six case studies.

#### 4.3.1 LST Standardization Procedure

Technically, standardization of the LST raster datasets means determining by how many standard deviations (SD) is the LST value of every single pixel in each of the selected cases below or above mean LST value of the whole LST sample. The whole LST sample means all the LST pixels in each of the six gridded LST datasets that fall within the administrative border of Krakow. Standard scores of the land surface temperatures ($LST_S$) were calculated by subtracting the zonal mean LST value for the whole LST sample ($LST_\mu$) from an individual LST pixel value ($LST_x$) in each of the gridded LST datasets and dividing by the sample's standard deviation ($LST_\sigma$), which was also calculated for the whole LST sample:

$$LST_S = \frac{LST_x - LST_\mu}{LST_\sigma} \tag{10}$$

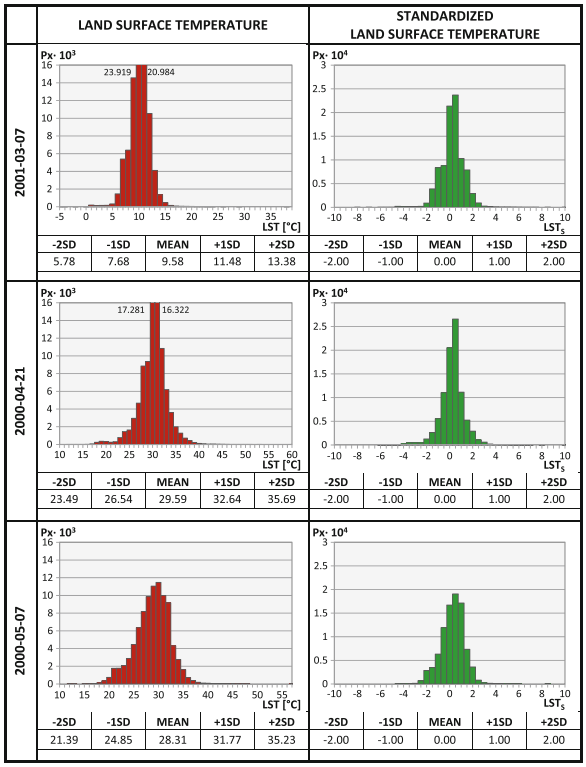


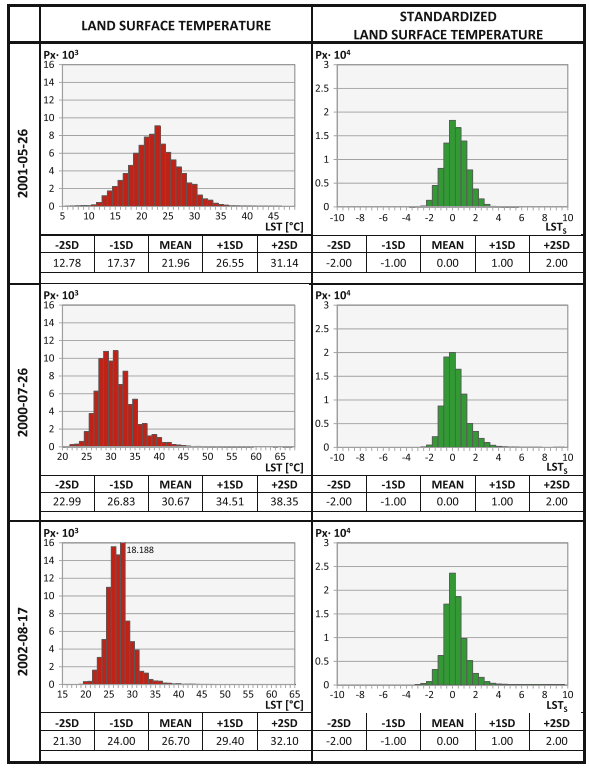


Figure 6
Comparison of LST and $LST_S$ distributions

The LST distributions for the selected case studies were close to normal so there was no need to transform input data. After standardization, the distribution of each $LST_S$ variable is characterized by an expected value (mean) equal to 0 and a SD equal to 1 (Fig. 6).

The spatial extent of the LST sample was restricted to the administrative border of Krakow because in this study the focus was on delineating the thermal regions within Krakow's urban areas. Such restriction is acceptable as long as the proportion between artificial and semi-natural surfaces is more or less equal within the area of Krakow (Fig. 4), as the method is sensitive to zonal mean and standard deviation values (Eq. 10).

#### 4.3.2 *Delimitation of Thermal Regions*

A set of maps showing standardized LST pattern in the agglomeration of Krakow for each of the six case studies was created. Furthermore, for each standardized land surface raster dataset, local functions of raster analysis were used in order to calculate the frequency of $LST_S$ pixels. Thermally stable regions [with $LST_S$ always (6/6 case studies) higher or always lower than the zonal mean $LST_\mu$ of Krakow] were determined. Additionally, the stable hot regions and stable cold regions were divided according to the strength of the thermal stability into three categories (spots) defined by a number of standard deviations. Pixels classified sometimes as hot and sometimes as cold, depending on a date, were considered as unstable (Table 5). Local raster analysis tools (map algebra, reclassification, local statistics) available in ArcGIS Desktop Spatial Analyst were used to delineate thermal regions. A map of thermal regions in the agglomeration of Krakow was created. Seven most characteristic cold and hot spots were analyzed.

#### 4.3.3 *Spatial Analysis of Standardized Land Surface Temperature*

Zonal statistics were calculated in order to examine the relationship between standardized LST patterns and land cover types within administrative border of Krakow. Two quantifiers were introduced: mean standardized LST for the defined land cover classes and percentage share of the hot and cold spots in each of defined land cover class. The CLC2000 dataset was used instead of the GMES Urban Atlas because the minimum mapping unit of the GMES land cover dataset (0.25 ha) is too small and some of the elements, e.g. linear objects such as roads, are too narrow with respect to the 60-m resolution of the LST raster datasets and are for that reason inappropriate for calculation of the zonal statistics.

## 5. *Results*

### 5.1. *Case Studies*

The six selected images represent various stages of the vegetative period. LST in the area of Krakow is greatly diversified into what can be clearly seen in the maps (Fig. 7). Two main centers of very high heat emission can be distinguished. These are: Krakow city center and the steelworks in Nowa Huta with the whole industrial infrastructure (compare Figs. 1c, 7, Fig. 8). The temperature higher than the average mean value for Krakow regardless of season and

Table 5

*Categories of thermal regions and strength of thermal stability*

| Thermal region | Category of thermal stablity | Thermal spot name |
|---|---|---|
| Stable hot | 6/6 → >2 SD | very hot spot |
| | 6/6 → >1 SD | hot spot |
| | 6/6 → 0–1 SD | warm spot |
| Unstable | Diversified | |
| Stable cold | 6/6 → −1–0 SD | cool spot |
| | 6/6 → ≤−1 SD | cold spot |
| | 6/6 → ≤−2 SD | very cold spot |

*SD* standard deviation, 6/6 means that a certain pixel was classified to the same category in all 6 analyzed images

atmospheric conditions can be also observed in areas occupied by other, smaller factories and industrial units as well as huge shopping centers. On the other hand, the Vistula river, surface water reservoirs, forests, bigger city parks and wooded cemeteries (Figs. 2, 5) are generally characterized by much lower temperatures than the average, and for that reason are also easily recognizable in the maps. The temperature of the areas with other types of land use shows seasonal variability. Specifically, the thermal properties of arable land vary seasonally.

On March 07, 2001, the role of a particular land cover type in controlling the surface temperature was additionally modified by snow, which covered the upland located in the northern part of the study area. Another interesting aspect refers to the temperature of the rural areas located to the northeast of the city. In spring (images April 21, 2000; May 07, 2000 and May 26, 2001), the thermal contrast between this region and the city of Krakow is very small. The LST is nearly the same as in the city center or in the area of steelworks. This effect is driven by intensive agriculture, which developed in this region due to high soil fertility and very good climate conditions. There are almost no forests. The area is generally used for vegetable cultivation and in spring the plant cover is relatively sparse yet. Consequently, the bare soil surface exposed to solar radiation warms up very quickly. The thermal contrast between the city and the surroundings increases as the plant cover gets denser (July 26, 2000) and then blurs again after harvest (August 17, 2002).

Thermal contrast between the city and the surroundings was mostly visible on July 26, 2000, when air temperature was also the highest (about 25 °C at the time of image acquisition). The reason for that was greater heat storage of urban surfaces during a sunny and very warm summer day because of specific thermal properties (i.e. heat capacity and conductivity) of man-made materials. In addition, heat accumulation in the city is also caused by the complex 3-dimensional nature of the urban surface, especially within the continuous urban fabric as a consequence of daytime radiative surplus of street canyon structure energy balance. Moreover, emission of anthropogenic heat from industrial and communal processes may strengthen the effect. This, however, plays a more significant role in winter time.

Detailed analysis of the relationship between the standardized LST and land cover types (Table 6) shows that the LST of urban fabric, industrial and commercial areas, as well as airport and large railway areas is always (6/6) higher than the zonal mean LST in Krakow. Continuous urban fabric is the warmest land cover class with mean standardized LST greater than 1.3 SD for each case, excluding May 26, 2001 (mean $LST_S = 0.99$ SD). The LST values in this class are very high (mean $LST_S > 2.2$ SD), particularly during hot summer days (July 26, 2000 and August 17, 2002). The strong overheating in this class is caused most of all by very high heat capacity of predominant artificial surfaces such as asphalt, concrete and roof sheeting, but also a very small share of vegetation. More vegetation (urban greenery) can be found in between discontinuous urban fabric and, therefore, the temperature is lower ($0.10$ SD $<$ mean $LST_S < 0.61$ SD). Interestingly, industrial and commercial areas are not the warmest, although the maps prove that the hottest pixels are linked with metallurgical furnaces, factory chimneys and large, flat roofs of hypermarkets or industrial buildings. The mean temperature ($0.46$ SD $<$ mean $LST_S < 1.13$ SD) is, however, lower than in the case of continuous urban fabric mainly because of the vegetation contribution and heterogeneity of buildings.

The LST values of forests and waters are always much lower than the zonal mean LST in Krakow, especially in a warm part of the year. Before the vegetative period (March 7, 2001) waters (mean $LST_S = -1.84$ SD) are significantly colder than forests (mean $LST_S = -0.63$ SD); then, in early growing season (May) the forests ($-1.75$ SD $<$ mean $LST_S < -1.61$ SD) are colder than waters ($-1.58$ SD $<$ mean $LST_S < -0.94$ SD), whereas in late growing season (July and August), the mean temperature of surface waters and forests is nearly the same ($LST_S$ about 1.2–1.5 SD lower than the zonal mean LST in Krakow). This temperature variation is caused by annual vegetation and air temperature changes linked to evapotranspiration, which is more intensive in the phase of maximum vegetation growth and also when the air temperature increases. The LST of green urban areas is not much lower (mean $LST_S$ from $-0.40$ to $0.11$ SD) than the zonal mean LST in Krakow, regardless of the time of year.

The temperature of arable land, meadows, pastures, permanent crops and horticulture shows large seasonal changes. These land cover classes may contribute to the increase but also the decrease of the overall mean surface temperature in the city depending on a season. The temperature of arable land is a little bit higher than the mean (0.07 SD $<$ mean $LST_S$ $<$ 0.18 SD) only during the early vegetative season, while the temperature of grassland (mean $LST_S = 0.38$ SD), permanent crops and horticulture (mean $LST_S = 0.05$ SD) is higher before the vegetative period (Mar 7, 2001). The reason for this difference lies in keeping the arable land uncovered for some time after planting crops on the ploughed fields in the first phase of the vegetative period (April–May). Accordingly, at that time, thermal properties of the arable land are similar to bare soil, i.e. it heats up faster than the soil covered with vegetation.

### 5.2. Thermal Regions

The map of thermal stability in the agglomeration of Krakow (Fig. 8) shows that hot regions (defined as in Table 5) are located most of all in the city center, along main arterial thoroughfares and industrial zones (primarily Nowa Huta steelworks and related infrastructure). The three satellite towns of Skawina, Wieliczka and Niepolomice (see Fig. 1) are also clearly seen.

The cold regions (defined as in Table 5) correspond to the areas of forests, city parks and water reservoirs. Thanks to the application of shaded relief in the background of the map and making the upper thermal regions layer 50 % transparent, it can be noticed that many cold regions are also located on the northern slopes of the Carpathian Foothills. The reason for this effect is a nearly-constant illumination angle (sun azimuth around 150°) during satellite acquisition of all the six Landsat/ETM+ images used in the study.

A percentage share of cold and hot areas related to defined standard deviation thresholds for all the land cover types within the city of Krakow was calculated (Table 7). Generally, about 1/3 (32.4 %) of the total city area is thermally stable. Approximately half (16.6 %) of the thermally stable areas is always warmer and the other half (15.8 %) of the area is always colder than the mean zonal LST for Krakow. The most thermally stable and the warmest land cover class is continuous urban fabric. Of the area covered by the continuous urban fabric, 92 % is always warmer than the mean zonal LST for Krakow. The hot spots (>1 SD) represent almost 50 % of the area in this class. The biggest amount of very hot spots (>2 SD) falls within industrial and commercial areas, although a general number of pixels warmer than the mean zonal LST is only about 50 % in this class. The other classes with a definitely higher number of always warm pixels (>AVG) are: airport and large railway areas (60.5 %) and discontinuous urban fabric (about 32 %). Forests and waters are the most thermally stable and the coldest classes. Forests consist of the largest number of cold pixels—nearly 80 % area in this class is colder than the mean zonal LST. On the other hand, waters are locally much colder than forests. Two percent of water pixels are classified as very cold spots (<−2 SD), whereas pixels in this category do not exist at all in the forest class.

Characteristic thermal regions located in Krakow were identified and marked in the map (Fig. 8) with dotted rectangle polygons. The hot and cold regions are easily distinguishable (with characteristic pattern), and thermally stable [with LST values always (6/6) higher or lower than the mean LST for Krakow] places. Four interesting hot regions and three cold ones were recognized. Those seven areas were clipped from the map of thermal regions, draped over true color RGB composites of high-resolution orthophotomaps with the same 50 % transparency and comprehensively investigated (Figs. 9, 10, 11, 12, 13, 14, 15).

The selected cold and hot regions are:

*Water reservoirs in former gravel excavation sites in Przylasek Rusiecki* are old surface mine sites located in the Vistula River valley where gravel was excavated for the needs of the steelworks construction in Nowa Huta. Once the mining ceased, the pits naturally filled with water. The total area of the reservoirs is 86.7 ha. They now serve as a recreation site giving the possibility of fishing, swimming and sunbathing. The reservoirs are separated by dikes covered with lush vegetation. The whole complex is

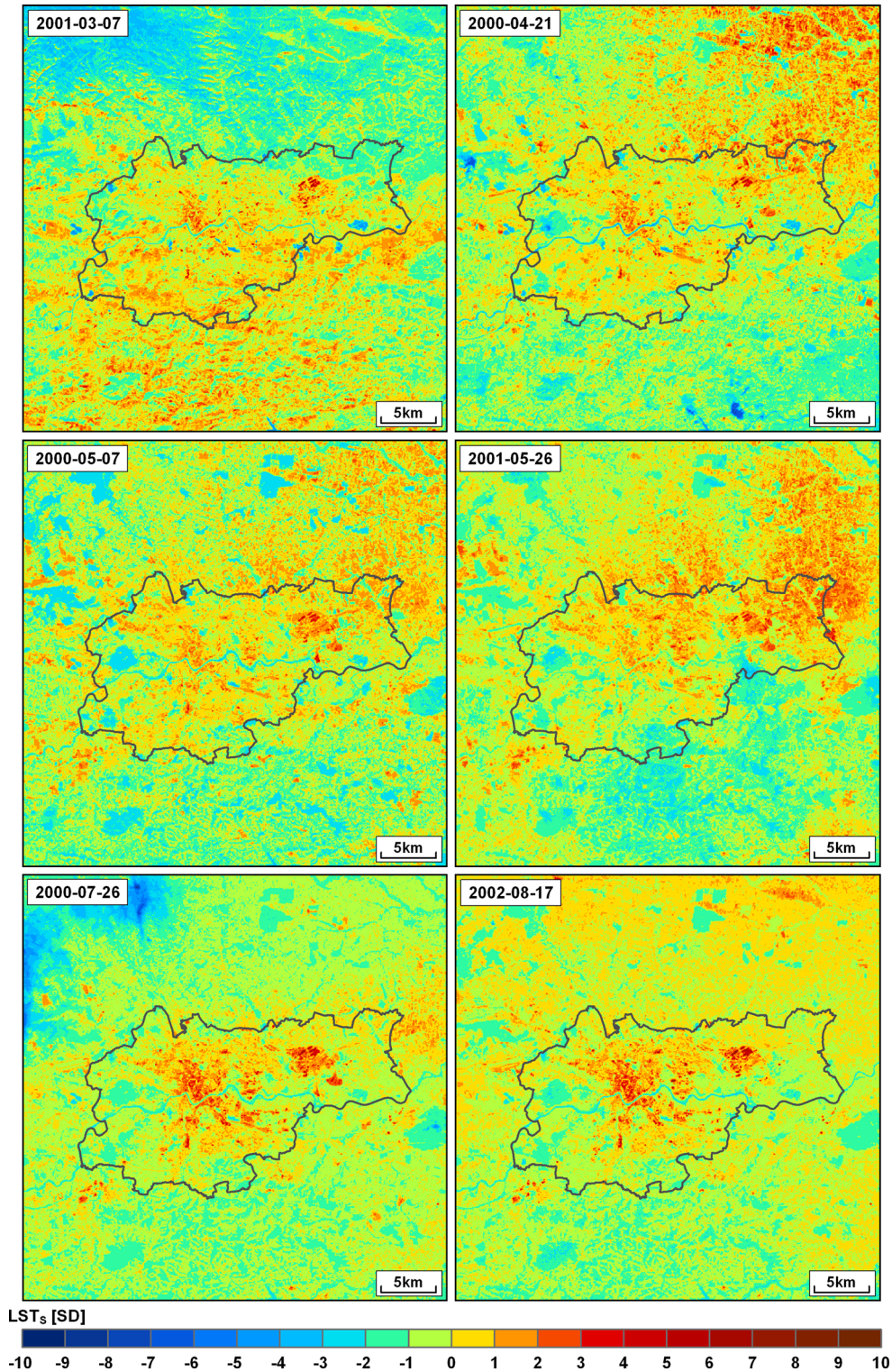


Figure 7
Standardized land surface temperature pattern in the agglomeration of Krakow

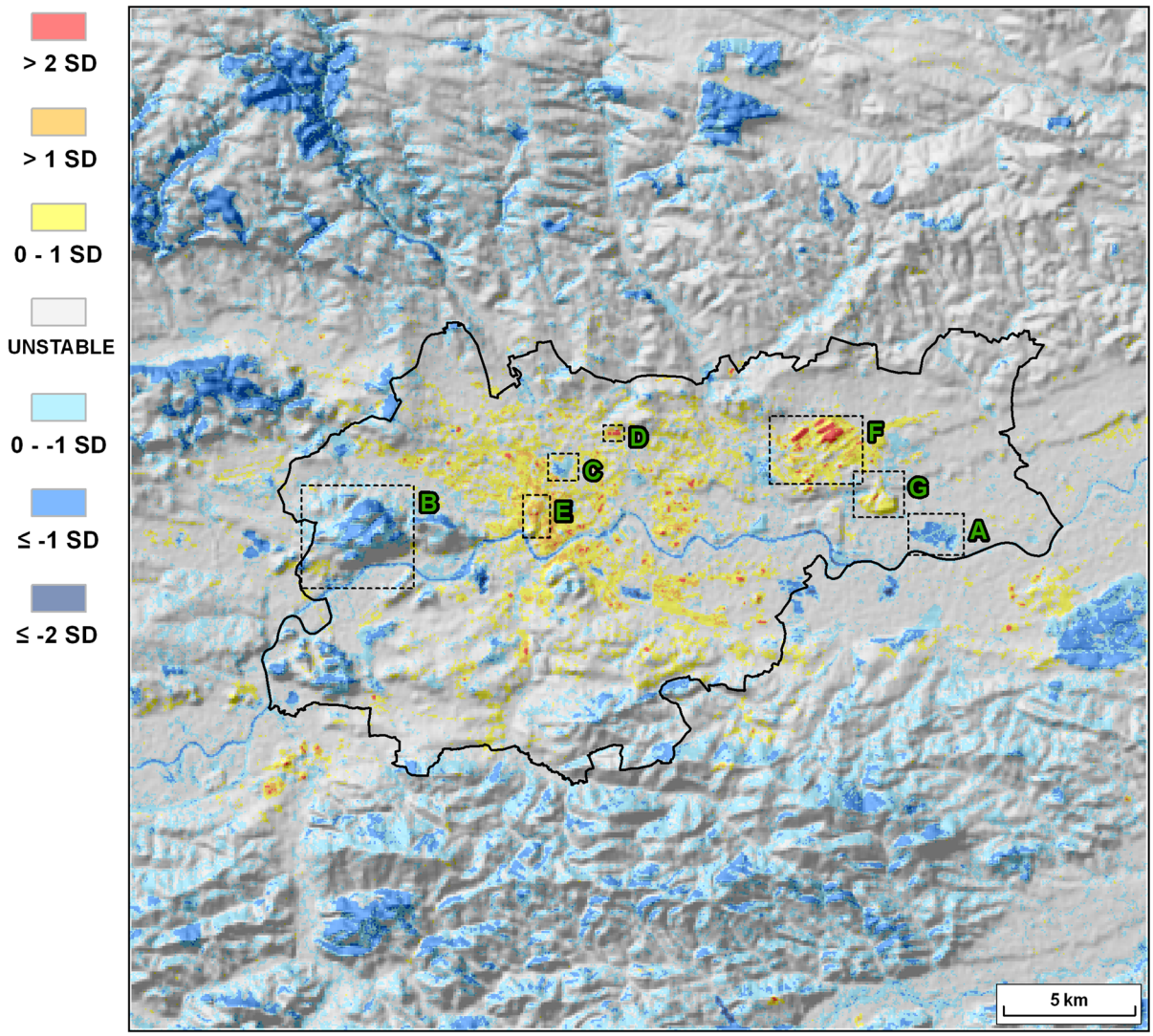


Figure 8
Thermal stability in the agglomeration of Krakow (*shaded relief in the background*). Characteristic cold and hot spots: **a** water reservoirs of former gravel excavation sites in Przylasek Rusiecki, **b** Wolski Forest, **c** Rakowicki Cemetery, **d** "Krokus" Shopping Center, **e** Krakow Old Town, **f** steelworks in Nowa Huta, **g** slag heap in Pleszow. Explanations of the colors in Table 6

surrounded by arable land, grassland and scattered single-family houses.

The 60-m resolution of the Landsat ETM+ thermal band is good enough to recognize the reservoirs and broader dikes (Fig. 9). Most of the reservoirs were identified as the cold spots. The rest of them and the dikes are cool spots.

*The Wolski Forest* is the largest forest complex within the administrative border of Krakow, with an area of 422 ha and very diversified landscape. The forest grows on a hill that is a tectonic horst built of Upper Jurassic limestone. Height differences reach up to 120 m, the slopes are steep, and the valleys are deep ravines. The Wolski Forest stand is a relatively natural composition of upland species dominated by oak, beech and birch trees. This natural site functions as a "green lung" of Krakow but also provides many touristic attractions.

The coldest spots in this subset area are the Vistula River and the northern slopes of the hill

Table 6

*Mean standardized land surface temperature (SD) inside the city limits for selected cases*

| Land cover class | Mar 7, 2001 | Apr 21, 2000 | May 7, 2000 | May 26, 2001 | Jul 26, 2000 | Aug 17, 2002 |
|---|---|---|---|---|---|---|
| Continuous urban fabric | 1.40 | 1.49 | 1.31 | 0.99 | 2.21 | 2.37 |
| Discontinuous urban fabric | 0.10 | 0.12 | 0.27 | 0.32 | 0.61 | 0.60 |
| Industrial and commercial areas | 0.46 | 0.67 | 0.85 | 0.80 | 1.13 | 0.97 |
| Airport and large railway areas | 0.50 | 1.09 | 0.98 | 0.82 | 0.94 | 0.67 |
| Green urban areas | −0.11 | −0.40 | −0.36 | −0.33 | −0.26 | −0.22 |
| Arable land | −0.31 | 0.18 | 0.07 | 0.11 | −0.30 | −0.21 |
| Meadows and pastures | 0.38 | −0.14 | −0.47 | −0.58 | −0.68 | −0.60 |
| Permanent crops and horticulture | 0.05 | −0.18 | −0.10 | −0.20 | −0.25 | −0.23 |
| Forests | −0.63 | −1.44 | −1.75 | −1.61 | −1.25 | −1.43 |
| Waters | −1.84 | −2.25 | −1.58 | −0.94 | −1.29 | −1.48 |

Land cover types as in Fig. 5

covered by the Wolski Forest (Fig. 10). Forest covering southern slopes descending towards the Vistula River valley was classified as thermally unstable. An apparent warm spot in the southwestern part of the subset area is generated by a housing estate of Bielany and another one at the eastern edge, north of the Vistula River, is a part of a similar housing estate in Przegorzaly. Two hot pixels located in the northwestern part of the subset area correspond to an industrial area (fuel base).

*The Rakowicki Cemetery* is one of the biggest and oldest cemeteries in Krakow with total area of 42 ha.

Here the thermal response of the surface is related to canopy structure, mainly the thickness of a tree crown layer. The southern, older part of the cemetery, especially its central divisions, which is densely forested (the canopy is thicker), form a cold spot. The rest of the cemetery has on average a bit higher temperature, however it remains thermally stable–cool. As the whole Rakowicki cemetery, located in the center of Krakow, is surrounded by a dense urban fabric, the neighboring area is stable–warm. The hottest spot in the southwestern part comes from a military area adjacent to a large road junction. The other hot spot located north of the cemetery is a commercial area with some warehouses (Fig. 11).

*"Krokus" Shopping Center* has a total area of 30,000 $m^2$. It consists of one huge hypermarket, 53 boutiques and service points, two mid-surface stores and 1,500 parking places. The other smaller building to the west of the "Krokus" Center is a construction hypermarket. Both buildings formed very distinctive hot spots. There are many restaurants, smaller shopping, service and entertainment centers around. A part of the two-lane northern bypass of Krakow is also included in the southern part of this subset area. A semicircular, multi-leveled roof of an aqua park, which can be seen in the northeastern part of this subset image, heats up unevenly and not as strongly as the roof of the shopping centers (Fig. 12).

This thermal region is a good example of how the shape and color of the roof, its area, and the type of material it is made of can influence thermal properties. Almost the whole site consists of different artificial surfaces with low albedo and high heat storage potential. More vegetation can only be found around blocks of flats located in the northwestern and southern part of this subset area. These two places were classified as thermally unstable.

*Krakow Old Town with the Wawel Royal Castle (UNESCO World Heritage Site)* comprises Krakow's historical center surrounded by a park called the Planty. The characteristic urban structure of the Old Town consists of the Main Market Square with dimensions of 200 m × 200 m in the central point, and the entire old town is divided into quarters, separated by a regular grid of streets. The Wawel Castle is located in the south of the Old Town, on a hill at the Vistula River (Fig. 13).

The regular urban structure of the Old Town delimited by a green belt can be found in the LST pattern. The entire central city district is characterized with a very high LST. An included small part of the Vistula River is the only cold spot. Planty Park, in its western, broader section is locally stable–cool. Wawel hill slopes, the Main Market Square, and the

Table 7

*Percentage share (%) of hot and cold areas in different land cover types within the city administrative border*

| Land cover class | >AVG | >1 SD | >2 SD | <AVG | <−1 SD | <−2 SD |
|---|---|---|---|---|---|---|
| Continuous urban fabric | 92.0 | 46.6 | 1.3 | 0.6 | 0.0 | 0.0 |
| Discontinuous urban fabric | 31.9 | 2.2 | 0.1 | 6.2 | 0.3 | 0.0 |
| Industrial and commercial areas | 49.9 | 12.4 | 3.1 | 4.4 | 0.6 | 0.1 |
| Airport and large railway areas | 60.5 | 12.1 | 1.0 | 2.8 | 0.4 | 0.0 |
| Green urban areas | 7.1 | 0.1 | 0.0 | 32.5 | 3.7 | 0.0 |
| Arable land | 2.3 | 0.0 | 0.0 | 9.0 | 0.4 | 0.0 |
| Meadows and pastures | 2.0 | 0.0 | 0.0 | 18.3 | 2.6 | 0.0 |
| Permanent crops and horticulture | 6.7 | 0.1 | 0.0 | 16.6 | 0.8 | 0.0 |
| Forests | 0.2 | 0.0 | 0.0 | 79.0 | 32.3 | 0.0 |
| Waters | 1.1 | 0.0 | 0.0 | 77.4 | 41.0 | 1.7 |
| Krakow | 16.6 | 2.6 | 0.4 | 15.8 | 3.2 | 0.1 |

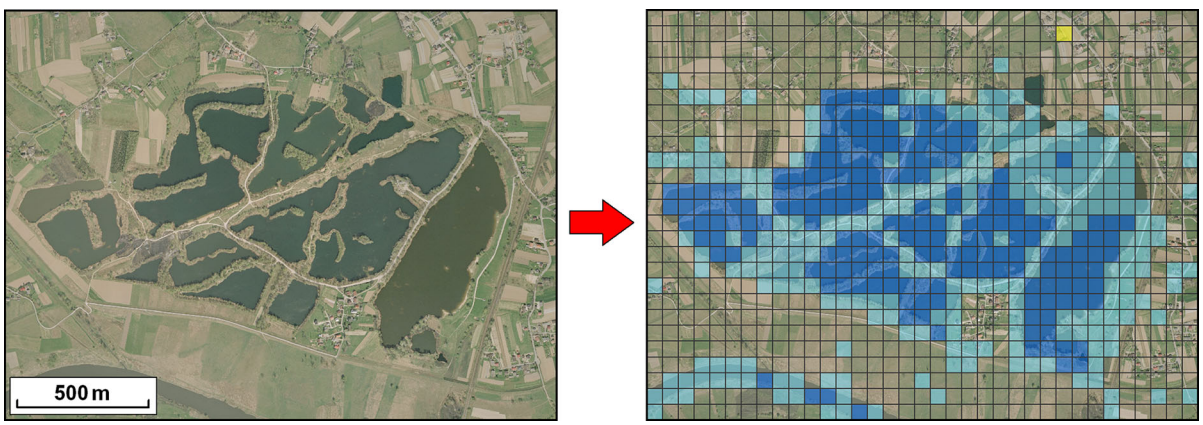


Figure 9
Thermal pattern of water reservoirs in former gravel excavation sites in Przylasek Rusiecki. Explanations of the colors in Table 5

Planty as well as two inner-city monastic gardens located in the northwestern and southeastern part of the area are thermally unstable.

*Steelworks in Nowa Huta (currently ArcelorMittal Poland, Krakow Branch)* are the second largest steelworks in Poland, producing annually about 1.3 million tons of steel and employing about 3,500 people.

The thermal pattern in this area (Fig. 14) corresponds to the location of different factory buildings, but it is also related to the industrial activity of the steelworks. The four large, very hot spots in this subset correspond to four large buildings of different rolling mills. The biggest one is a hot strip mill with a separate service center, the smallest one is a pipe rolling mill and the remaining two are cold rolling mills. The other smaller hot pixel clusters and singular hot pixels in this subset area are "produced" by other industrial plants located within the steelworks area, e.g.: a refractory materials plant, steel foundry, coke plant, and blister steel plant. There are two thermally unstable parts surprisingly located in the places of the most essential components of the steelworks:

- Blast furnaces located in the center of the steelworks area (south of the major hot spot of combined buildings of the hot strip mill and the service center).
- Sinter plants located in the very southeast of the subset area.

Spectral response from these industrial plants was interrupted by smoke clouds, which were released into

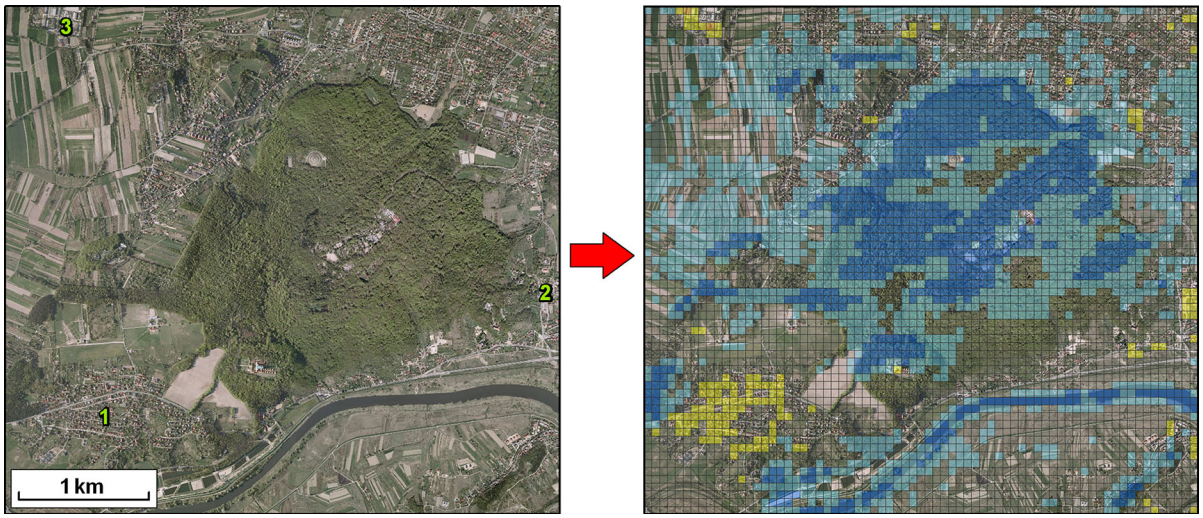


Figure 10
Thermal pattern of Wolski Forest and the surroundings: *1* housing estate of Bielany, *2* housing estate of Przegorzały, *3* industrial area of ORLEN fuel Base. Explanations of the colors in Table 5

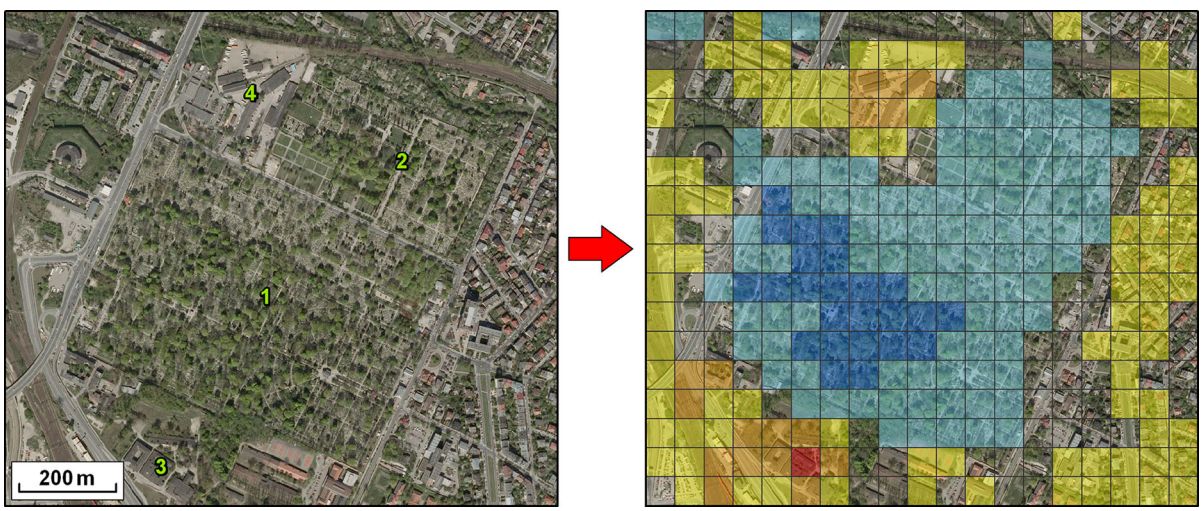


Figure 11
Thermal pattern of Rakowicki Cemetery and the nearest surroundings (*1* old cemetery, *2* new cemetery, *3* military area, *4* commercial area). Explanations of the colors in Table 5

the atmosphere with different intensity in five out of six images used in this research. The artificial atmospheric effect from those plumes likely affected the atmospheric correction for the respective pixels. As the steelworks is separated from the rest of the city with a green protective zone, some cold pixels are also visible in the western and southeastern parts of the subset.

*Slag heap in Pleszow with its entire infrastructure* is a dump site located south of the steelworks and occupying about 156 ha. It is still stored with the steelworks slag waste (a vitreous byproducts of steelmaking). The previously accumulated material is nowadays excavated for further use, e.g. road construction. The LST of almost the whole heap

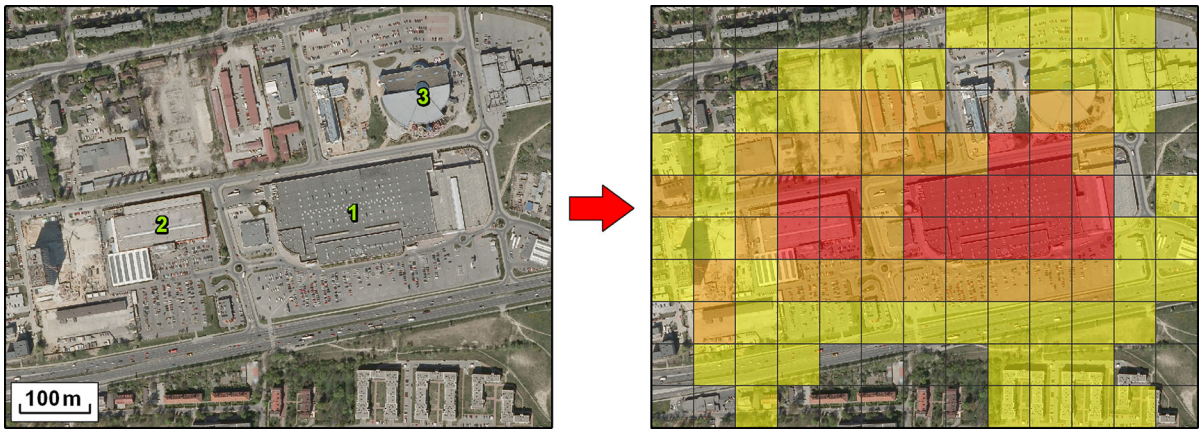


Figure 12
Thermal pattern of "Krokus" Shopping Center (*1*) and the neighboring construction hypermarket (*2*) and aqua park (*3*). Explanations of the colors in Table 5

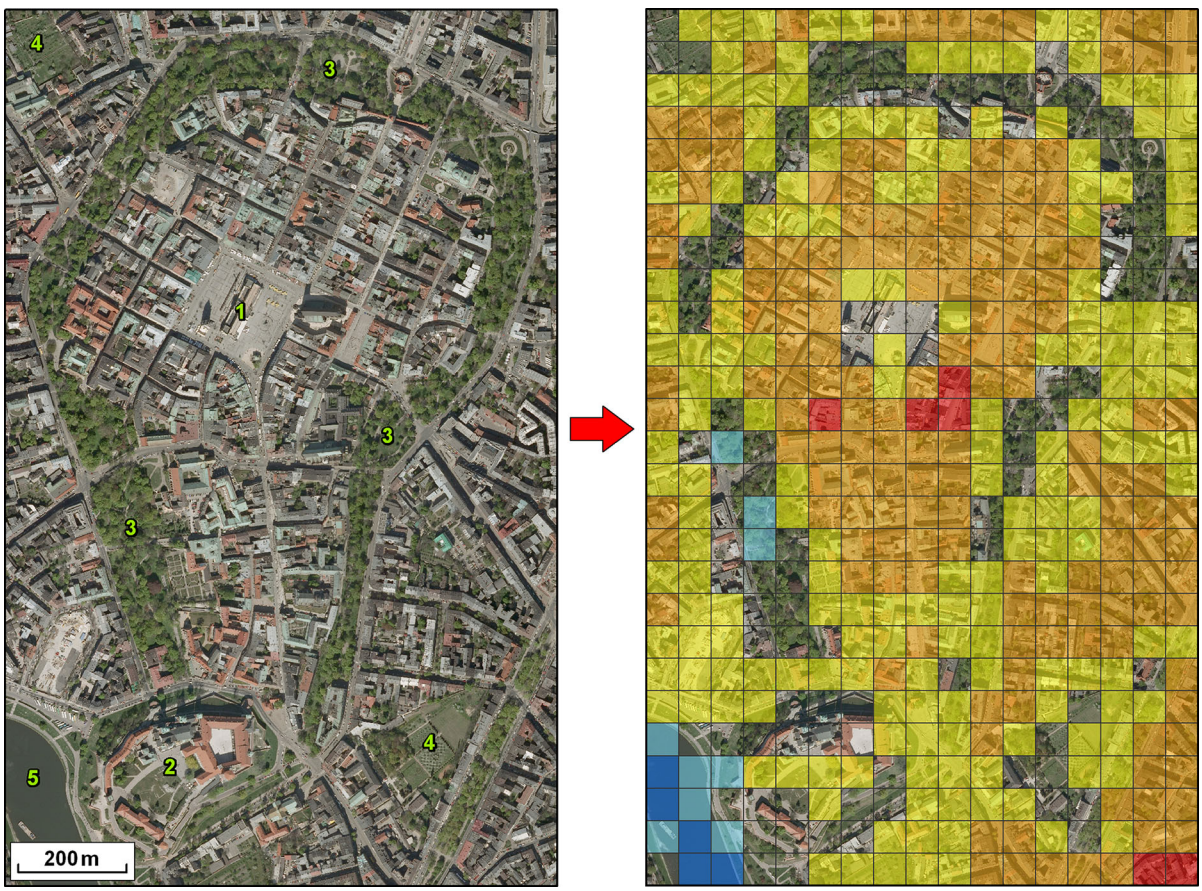


Figure 13
Thermal pattern of the Old Town in Krakow (*1* Main Market Square, *2* Wawel Castle, *3* Planty Park, *4* monastic gardens, *5* Vistula river). Explanations of the colors in Table 5

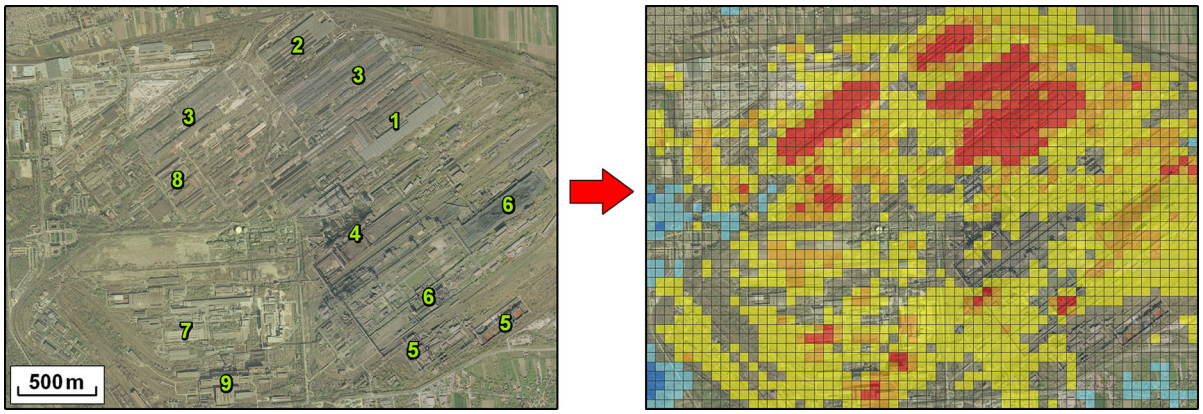


Figure 14
Thermal pattern of the steelworks in Nowa Huta (*1* hot strip mill, *2* pipe rolling mill, *3* cold rolling mills, *4* blast furnaces, *5* sinter plants, *6* coke plant, *7* refractory materials plant, *8* steel foundry, *9* blister steel plant). Explanations of the colors in Table 5

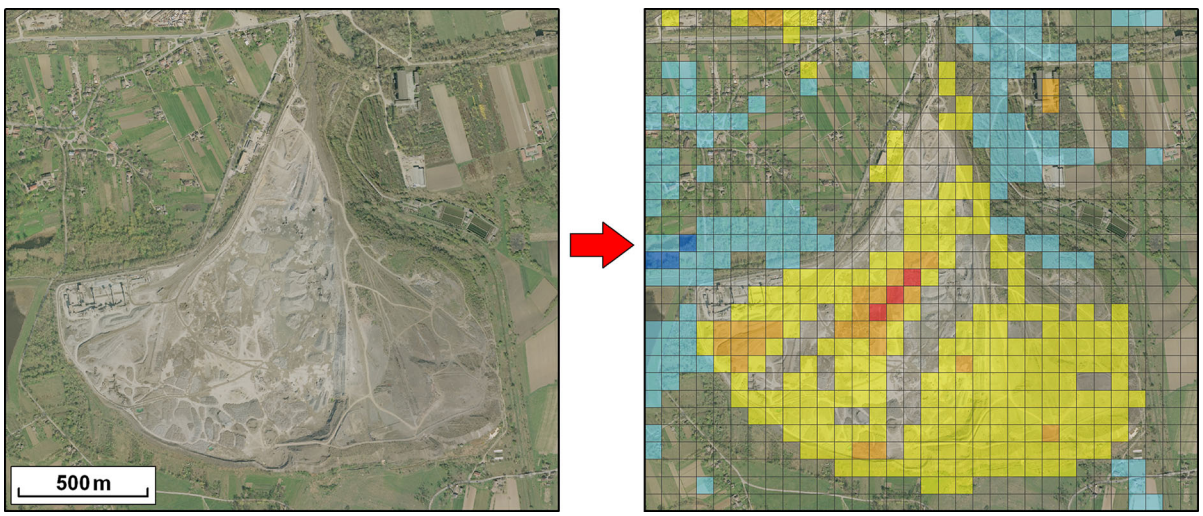


Figure 15
Thermal pattern of the slag heap in Pleszow. Explanations of the colors in Table 5

area is higher than the average LST in Krakow, but pixels related to infrastructure located within the heap are hotter. The three very hot pixels correspond most probably to the place where in the years 2000 and 2001 liquid slag was poured from the special cars and cooled off over a few days (Fig. 15).

It has to be clarified that as the thermal regionalization was based on the six $LST_S$ raster datasets, it shows only overall tendency in spatial distribution and seasonal variability of LST. For exhaustive analysis, more satellite images should be included.

## 6. Summary and Conclusions

This paper contains detailed evaluations of the LST distribution in the agglomeration of Krakow, located in southern Poland. The LST records were obtained from six Landsat/ETM+ multispectral images with the use of a single-channel algorithm. The method employs atmospheric and emissivity correction. Standardization of the LST values enabled an objective comparison of spatial distribution of the LST values derived from images acquired in different atmospheric conditions and in various phases of the vegetative period. Furthermore, recognition of

thermally characteristic regions in the LST pattern was possible. The method is universal and can be applied with no limitations given selection of a proper reference area where proportions of natural and artificial surfaces are equalized and the statistical distribution of LST pixels tend to be normally distributed. Further processing included calculation of zonal statistics in order to evaluate the relationship between standardized LST and different land cover types. All data processing procedures applied in this study have been performed automatically within the GIS environment. GIS is a powerful tool which enables implementation of LST retrieval and standardization procedures as well as integration of created standardized LST maps with other geospatial data (e.g. land cover database).

The results confirmed that the LST pattern depends most evidently on thermal properties (such as heat capacity and conductivity) of different surfaces. In Krakow, as well as in other urban areas, LST pattern is influenced by both environmental and anthropogenic factors. Various natural and artificial surfaces form characteristic mosaic structures, which result typically in great spatial variability of LST. Created maps of LST highlighted some peculiarities of the LST pattern in the agglomeration of Krakow, which are related to the specific urban structure of the city as well as to the location of the whole urban area in the bottom of the Vistula River valley in between the Malopolska Upland and the Carpathian Foothills. There are two easily distinguishable places of the highest surface temperature regardless of season and prevailing weather conditions: the city center (mostly continuous urban fabric) and the whole industrial area of steelworks in Nowa Huta. Smaller factories and industrial units as well as huge shopping centers are also always characterized by very high LST. Continuous urban fabric is on average the warmest land cover class, but the most extreme LST values occur within industrial and commercial areas. This is caused by the heat accumulation capacity of artificial surfaces and the emission of anthropogenic (industrial and communal) heat. Forests, bigger city parks, wooden cemeteries and waters are always the coldest areas. Waters are locally much colder than forests especially in the non-vegetative period. The temperature of the areas with other types of land use (especially arable land) shows seasonal variability.

The exact temperature difference describing strength of the thermal contrast is not easy to compute because it is difficult to define the background LST value. In this study, mean zonal LST within the administrative border of Krakow was used as the background temperature value. Thermal contrast between the city and the surroundings depends on a season, weather conditions and is the highest during hot, summer days.

Thermally stable regions have been identified on the basis of relationship between pixel $LST_S$ value and the zonal mean LST for Krakow ($LST_\mu$): hot region ($LST_S > LST_\mu$), cold region ($LST_S < LST_\mu$). Pixels classified sometimes as hot and sometimes as cold, depending on a date, were considered as unstable. The research showed that about one-third of the total city area is thermally stable. More than 16 % of the city is always warmer and less than 16 % is always colder than the $LST_\mu$. Hot and cold regions are not evenly distributed in the city. Seven characteristic hot and cold regions located within the Krakow administrative limits were selected and comprehensively investigated, taking into consideration the strength of thermal stability divided by a number of standard deviations.

According to the results obtained, LST in Krakow and its vicinities is influenced by four major factors:

- *Land cover type* LST pattern corresponds to the extent of different land cover types, which is a consequence of different thermal properties of surfaces (conductivity and capacity);
- *Vegetation cycle* causes seasonal changes of thermal properties of particular land cover classes, e.g. forests, green urban areas, arable lands, meadows and pastures or permanent crops and horticulture;
- *Land relief and building structure* insolated slopes and parts of buildings are warmer whereas shadowed surfaces are colder, creating a positive daytime energy balance of street canyon structure;
- *Atmospheric conditions* thermal contrast between the city and the surroundings is more evident during hot, summer days.

Further research on the influences of topography, vegetation type, shape of buildings and different

anthropogenic materials on the LST values should be done with the use of remotely sensed data of higher spatial resolution and in situ measurements. Detailed evaluation of the relationship between the LST and weather conditions with the use of an objective methods are also necessary.

The main advantages of Landsat ETM+ data as a source of information on spatial distribution of LST in urban areas are a nearly 30-year-long series of freely available records and relatively high spatial resolution of thermal band (60 m), which allows for detailed analysis of the LST pattern in relationship with different land cover types (in the scale of buildings, streets, parks, watercourses, etc.). On the other hand, temporal resolution of 16 days excludes the possibility of studying LST changes in shorter periods and only one thermal band available makes it more difficult to retrieve accurate LST values. The results of this study as well as numerous other research activities employing a single-channel algorithm confirmed the high quality of the LST retrievals and the great potential of Landsat ETM+ data in terms of urban thermal environment research. However, taking into consideration the properties of the Landsat data (relatively high spatial resolution and long revisit time between observation of the same point on the Earth's surface), the primarily types of Landsat data research applications are case studies and change detection studies. Finally, it has to be noticed that the ETM+ sensor was fully operational only for 4 years (from April 1999 to May 2003). Hence, shortage of SLC-on and cloud-free Landsat ETM+ imagery is another considerable limitation for this kind of research. Even though some methods of filling the ETM+ image gaps caused by SLC failure were developed, the quality of a research based on not fully valuable data decreases considerably. Alternatively, Landsat TM data could be used, but the spatial resolution of the thermal band is two times lower. A new perspective for improvements in similar research activities in future has come with the recently launched (so far not damaged) Landsat-8 (LDCM) satellite with two separate sensors [Operational Land Imager (OLI) and Thermal Infrared Sensor (TIRS)] (NASA Landsat Data Continuity Mission Website 2013).

Universality of the method used in this research implies applicability to different environmental conditions worldwide. The results of this study can be a very supportive contribution for local municipal authorities and urban planners around the world in all kinds of actions towards neutralization of the negative effects of human activity on thermal conditions in urban areas. Standardization of the LST values not only makes it possible to retrieve LST patterns or delineate thermal regions on the basis of satellite images acquired in different environmental conditions, but also enables the identification of the processes behind them. This research used zonal statistics to study the relationship between LST and land cover, which can also be interpreted as an indirect measure of dynamic human-driven processes on the Earth's surface. Stable hot spots correspond most of all to continuous urban fabric as well as industrial and commercial areas where human activity is the highest. Permanent man-made transformation of the urban environment leading to, among other results, intensive production and accumulation of artificial heat is not easy to reverse. It is very difficult to restore greenery or surface waters in a dense urban structure, but not impossible. One of the more progressive solutions is the concept of so-called 'green roofs', which means covering existing buildings with greenery to stabilize thermal conditions in the city. This is an important aspect of sustainable urban development, which can improve the living standards of urban residents.



## References

ASTER Spectra Library available on-line: http://speclib.jpl.nasa.gov/, accessed in Oct. 2012.

Barsi, J. A., Barker, J. L., and Schott, J. R. (2003), *An Atmospheric Correction Parameter Calculator for a Single Thermal Band Earth-Sensing Instrument*, Proc. IEEE IGARSS, 21–25 July 2003, Toulouse, France, 3014–3016.

Barsi, J. A., Schott, J. R., Palluconi, F. D., and Hook, S. J. (2005), *Validation of a Web-Based Atmospheric Correction Tool for Single Thermal Band Instruments*, Earth Observing Systems X, Proc. SPIE, Vol. 5882, August 2005, Bellingham, WA.

Bielecka E., and Cioikosz, A., *CORINE Land Cover in Poland. Final report*, (Inst. of Geodesy and Cartography, Warsaw 2004; available on-line at: http://www.igik.edu.pl/images/stories/sip/clc_final_report_pl.pdf), accessed in Oct. 2012.

Bokwa, A., *Wieloletnie zmiany struktury mezoklimatu miasta na przykładzie Krakowa [Multi-annual changes of the urban mesoclimate structure using an example of Kraków]*, (Inst. of Geography and Spatial Management, Jagiellonian University, Krakow 2010) (in Polish, summary in English; available on line at: http://www.geo.uj.edu.pl/publikacje.php?id=000155&page=monografie&menu=3), accessed in Oct. 2012.

Bokwa, A., Sikora, S., and Szymanowski, M., *Topoklimatyczne zróżnicowanie temperatury powietrza na terenie Krakowa [Topoclimatic diversity of air temperature in Cracow]*, In Klimat i bioklimat miast [Urban climate and bioclimate] (ed. Kłysik, K., Wibig, J., and Fortuniak, K.) (University of Lodz, Lodz 2008), pp. 35-44 (in Polish, summary in English; available on line at: http://nargeo.geo.uni.lodz.pl/~meteo/stronki/stronki_klimatbio/monograph.pdf), accessed in Oct. 2012.

Carlson, T. N., Augustine, J. A., and Boland, F. E. (1977), *Potential application of satellite temperature measurement in the analysis of land use over urban areas*, Bull. Am. Meteorol. Soc. *58*, 1301–1303.

Carlson, T. N., and Ripley, D. A. (1997), *On the relation between NDVI, fractional vegetation cover and leaf area index*, Remote Sens. Environ. *62*, 241–252.

Chander, G., Markham, B.L., and Helder, D.L. (2009), *Summary of current radiometric calibration coefficients for Landsat MSS, TM, ETM+ and EO-1 ALI sensors*, Remote Sens. Environ. *113*, 893-903.

CORINE Land Cover Technical Guide—Addendum 2000, available on-line: http://www.eea.europa.eu, accessed in Oct. 2012.

Cristóbal, J., Jiménez-Muñoz, J. C., Sobrino, J. A., Ninyerola, M., and Pons, X. (2009), *Improvements in land surface temperature retrieval from the Landsat series thermal band using water vapor and air temperature,* J. Geophys. Res. *114*, D08103, doi: 10.1029/2008JD010616.

Demographic Yearbook of Poland (Central Statistical Office, Warsaw, 2012), available on-line: http://www.stat.gov.pl, accessed in Oct. 2012.

EEA Data and Maps, available on-line: http://www.eea.europa.eu/data-and-maps, accessed in Oct. 2012.

Gabor, P., and Jombach, S. (2009), *The relation between the biological activity and the land surface temperature in Budapest,* Appl. Ecol. Env. Res. *7*(3), 241-251.

Geoportal, website of the Head Office of Geodesy and Cartography of the Republic of Poland, available on-line: www.geoportal.gov.pl, accessed in Oct. 2012.

GMES—Mapping Guide for a European Urban Atlas v.1.01 (2010), available on-line: http://www.eea.europa.eu, accessed in Oct. 2012.

Hajto, M. (2009), *Badanie czasowo-przestrzennej struktury warunków termicznych terenów miejskich i pozamiejskich na podstawie danych satelitarnych [Investigation of temporal-spatial structure of urban and non-urban surfaces' thermal conditions on the basis of satellite data]*, Prace Geogr. IGiGP UJ *122*, 71–79 (in Polish, summary in English; available on-line at: http://www.pg.geo.uj.edu.pl/czytelnik/spis-tresci-zeszytow), accessed in Oct. 2012.

Irish, R., *Landsat 7 Science Data User Handbook* (NASA Goddard Space Flight Centre, Greenbelt, Md. 2003), available on-line: http://landsathandbook.gsfc.nasa.gov, accessed in Oct. 2012.

Jarvis, A., Reuter, H.I., Nelson, A., and Guevara, E. (2008), *Hole-filled SRTM for the globe Version 4*, available on-line from the CGIAR-CSI SRTM: http://srtm.csi.cgiar.org, accessed in Oct. 2012.

Jiménez-Muñoz, J. C., and Sobrino, J. A. (2003), *A generalized single-channel method for retrieving land surface temperature from remote sensing data,* J. Geophys. Res. *108* (D22), 4688, doi: 10.1029/2003JD003480.

Jiménez-Muñoz, J. C., Cristóbal, J., Sobrino, J. A., Sòria, G., Ninyerola, M., and Pons, X. (2009), *Revision of the Single-Channel Algorithm for Land Surface Temperature Retrieval From Landsat Thermal-Infrared Data*, IEEE Trans. Geosci. Remote Sens. *47*, 339–349, doi:10.1109/TGRS.2008.2007125.

Lewińska, J., Zgud, K., Baścik, J., and Wiatrak, W., *Klimat obszarów zurbanizowanych [Climate of urban areas]* (Inst. of Spatial and Communal Economy, Warszawa 1990) (in Polish, summary in English).

Lewińska, J., and Zgud, K. (1980), *Wyspa ciepła na tle zespołów urbanistycznych Krakowa [Heat island versus urban complexes of Krakow]*, Przegląd Geofizyczny *25*, 3–4, 283–294 (in Polish, summary in English).

Li, J.-J., Wang, X.-R., Wang, X.-J., Ma, W.-C. and Zhang, H. (2009), *Remote sensing evaluation of urban heat island and its spatial pattern of the Shanghai metropolitan area, China,* Ecol. Complex. *6*, 413–420.

Li, J., Song, C., Cao, L., Zhu, F., Meng, X., and Wu, J. (2011), *Impacts of landscape structure on surface urban heat islands: A case study of Shanghai, China*, Remote Sens. Environ. *115*, 3249–3263.

Li, S., Zhao, Z., Miaomiao, X., and Wang, Y. (2010), *Investigating spatial non-stationary and scale-dependent relationships between urban surface temperature and environmental factors using geographically weighted regression,* Env. Model. Soft. *25*, 1789–1800.

Lillesand, T., and Kiefer, R.. *Remote Sensing and Image Interpretation* (John Wiley and Sons, Inc., New York 2000).

Liu, L., and Zhang, Y. (2011), *Urban heat island analysis using the Landsat TM data and ASTER data: a case study in Hong Kong,* Remote Sens. *3*, 1535–1552, doi:10.3390/rs3071535.

Lo, C. P., Quattrochi, D. A., and Luvall, J. C. (1997), *Application of high-resolution thermal infrared remote sensing and GIS to assess the urban heat island effect,* Int. J. Remote Sens. *18*, 287–304.

Lougeay, R., Brazel, A., and Hubble, M. (1996*), Monitoring intra-urban temperature patterns and associated land cover in Phoenix, Arizona using Landsat thermal data,* Geocarto International *11*, 79–89.

Mackey, C. W., Lee, X., and Smith, R. B. (2012), *Remotely sensing the cooling effects of city scale efforts to reduce urban heat island*, Building and Environment *49*, 348–358.

Maucha, G., and Büttner, G., *Validation of the European CORINE Land Cover 2000 database,* in *Global Developments in Environmental Earth Observation from Space* (ed. Marçal A. R. S.) (Millpress, Rotterdam, 2006), pp. 449–457.

MODIS UCSB Emissivity Library, available on-line: http://www.icess.ucsb.edu/modis/EMIS/html/em.html, accessed in Oct. 2012.

Morawska-Horawska, M., and Cebulak, E. (1981), *Badania pionowego zasięgu miejskiej wyspy ciepła nad Krakowem [Studies on vertical range of Urban heat island above Krakow]*, Folia Geogr., Ser. Geogr.-Phys. *14*, 43–50 (in Polish, summary in English).

NASA's Earth Observatory Blue Marble—Next Generation Composite, available on-line: http://earthobservatory.nasa.gov/Features/BlueMarble/, accessed in Oct. 2012.

NASA Landsat Project Website, available on-line: http://landsat.gsfc.nasa.gov, accessed in Oct. 2012.

NASA Landsat Data Continuity Mission Website: available on-line: http://ldcm.gsfc.nasa.gov/, accessed in Feb. 2013.

Nichol, J. E. (1996), *High-resolution surface temperature patterns related to urban morphology in a tropical city: a satellite-based study,* J. Appl. Meteor. *35*, 135–146.

Oke, T. R., *Boundary Layer Climates, 2nd edition* (Methuen & Co., USA 1987).

Oltra-Carrió, R, Sobrino, J. A., Franch, B., and Nerry, F. (2012), *Land surface emissivity retrieval from airborne sensor over urban areas,* Remote Sens. Environ. *123*, 298–305.

Petrişor, A.-I., Ianoş, I., and Tălângă, C. (2010), *Land cover and use changes focused on the urbanization processes in Romania*, Env. Eng. Manag. J. *9*, 765–771.

Pongrácz, R., Bartholy, J., and Dezső, Z. (2010), *Application of remote sensed thermal information to urban climatology of Central European cities,* Phys. Chem. Earth *35*, 95–99.

Price, J. C. (1979), *Assessment of the urban heat island effect through the use of satellite data,* Mon. Weather Rev. *107*, 1554–1557.

Qin Z., Karnieli, A., and Berliner, P. (2001) *A mono-window algorithm for retrieving land surface temperature from Landsat TM data and its application to the Israel-Egypt border region*, Int. J. Remote Sens., vol. *22*, no. 18, 3719–3746.

Rodriguez-Galiano, V., Pardo-Iguzquiza, E., Sanchez-Castillo, M., Chica-Olmo, M., and Chica-Rivas, M. (2012), *Downscalling Landsat 7 ETM+ thermal imagery using land surface temperature and NDVI images*, Int. J. App. Earth Obs. Geoinf. *18*, 515–527.

Roth, M., Oke, T. R., and Emery, W. J. (1989), *Satellite-derived urban heat islands from three coastal cities and the utility of such data in urban climatology*, Int. J. Remote Sens. *10*, 1699–1720.

Rouse, J. W., Haas, R. H., Schell, J. A., and Deering, D. W. (1973), *Monitoring vegetation systems in the Great Plains with ERTS*, In 3rd ERTS Symposium (NASA SP-351 I), pp. 309–317.

Salisbury, J. W., and D'Aria, D. M. (1992), *Emissivity of terrestrial materials in the 8-14 μm atmospheric window,* Remote Sens. Environ. *42*, 83–106.

Schowengerdt, R., *Remote sensing. Models and methods for image processing*, *3rd edition* (Academic Press, London 2007).

Sobrino, J. A., Caselles, V., and Becker, F. (1990), *Significance of the remotely sensed thermal infrared measurements obtained over a citrus orchard*, ISPRS J. Photogramm. Remote Sens. *44*, 343–354.

Sobrino, J. A., and Raissouni, N. (2000), *Toward Remote Sensing methods for land cover dynamic monitoring. Application to Morocco,* Int. J. Remote Sens. *21*, 353–366.

Sobrino, J. A., Raissouni, N., and Li, Z.–L. (2001), *A comparative study of land surface emissivity retrieval from NOAA data,* Remote Sens. Environ. *75*, 256–266.

Sobrino, J. A., Jiménez-Muñoz, J. C., and Paolini, L. (2004), *Land surface temperature retrieval from Landsat TM 5,* Remote Sens. Environ. *90*, 434–440.

Sobrino, J. A., Jiménez-Muñoz, J. C., Sòria, G., Romaguera, M., Guanter, L., Moreno, J., Plaza, A., and Martínez, P. (2008), *Land surface emissivity retrieval from different VNIR and TIR sensors*, IEEE Trans. Geosci. Remote Sens. *46*, 316–327, doi: 10.1109/TGRS.2007.904834.

Stathopoulou, M., Cartalis, C., and Keramitsoglou, I. (2004), *Mapping microurban heat islands using NOAA/AVHRR images and CORINE land cover: an application to coastal cities of Greece*. Int. J. Remote Sens. *25*(12), 2301–2316.

Stathopoulou, M., and Cartalis, C. (2007), *Daytime urban heat islands from Landsat ETM+ and Corine land cover data: An application to major cities in Greece*, Solar Energy *81*, 358–368.

Stathopoulou, M., and Cartalis, C. (2009), *Downscaling AVHRR land surface temperatures for improved surface urban heat island intensity estimation*, Remote Sens. Environ. *113*, 2592–2605.

Streutker, D. R. (2002*), A remote sensing study of the urban heat island of Houston, Texas,* Int. J. Remote Sens. *23*, 2595–2608.

Struzik, P. (1998), *Zastosowanie informacji satelitarnej AVHRR/NOAA do badania zjawiska miejskiej wyspy ciepła [Application of the AVHRR/NOAA satellite information for urban heat island investigation],* Acta Univ. Lodz., Folia Geogr. Phys. *3*, 161–171 (in Polish, summary in English).

Tomlinson, C. J., Chapman, L., Thornes, J. E., and Baker, C. (2011), *Remote sensing land surface temperature for meteorology and climatology: a review,* Meteorol. Appl. *18*, 296–306.

Tran, H., Uchihama, D., Ochi, S., and Yasuoka, Y. (2006), *Assessment with satellite data of the urban heat island effects in Asian mega cities*, Int. J. Applied Earth Obs. Geoinf. *8*, 34–48.

Tucker, C.J. (1979), *Red and photographic infrared linear combinations for monitoring vegetation*, Remote Sens. Environ. *8*, 127–150.

UN-HABITAT Report, *State of the World's Cities 2008/2009—Harmonious Cities* (Earthscan, London, UK & Sterling, VA, USA, 2010).

UN-HABITAT Report, *State of the World's Cities 2010/2011—Bridging The Urban Divide* (Earthscan, London, UK & Sterling, VA, USA, 2012).

USGS Landsat Website, available on-line: http://landsat.usgs.gov, accessed in Oct. 2012.

Valor, E., and Caselles, V. (1996), *Mapping land surface emissivity from NDVI: Application to European, African and South American areas,* Remote Sens. Environ. *57*, 167–184.

Van de Griend, A. A., and Owe, M. (1993), *On the relationship between thermal emissivity and the normalized difference vegetation index for natural surfaces,* Int. J. Remote. Sens. *14*, 1119–1131.

Voogt, J. A., and Oke, T. R. (2003), *Thermal remote sensing of urban climates,* Remote Sens. Environ. *86*, 370–384.

Vukovich, F. M. (1983), *An analysis of the ground temperature and reflectivity pattern about St. Louis, Missouri, using HCMM satellite data,* J. Climate Appl. Met. *22*, 560–571.

Walawender, J. (2009), *Wykorzystanie danych satelitarnych LANDSAT i technik GIS w badaniach warunków termicznych miasta (na przykładzie Aglomeracji Krakowskiej) [Application of LANDSAT satellite data and GIS techniques for estimation of thermal conditions in urban area (using an example of Krakow*

*agglomeration)],* Prace Geogr. IGiGP UJ *122*, 81–98 (in Polish, summary in English; available on-line: http://www.pg.geo.uj.edu.pl/czytelnik/spis-tresci-zeszytow), accessed in Oct. 2012.

Walawender, J., and Hajto, M. (2009), *Assessment of thermal conditions in urban areas with use of different satellite data and GIS,* Proc. 2009 EUMETSAT Meteorological Satellite Conference, 21–25 September 2009, Bath, United Kingdom (available online: http://www.eumetsat.int/idcplg?IdcService=GET_FILE&dDocName=PDF_CONF_P55_S4_25_WALAWEND_P&RevisionSelectionMethod=LatestReleased).

Walawender, J., Hajto, M., and Iwaniuk P. (2011), *Zastosowanie algorytmu „pojedynczego okna" do opracowania map temperatury powierzchni Ziemi na podstawie danych satelitarnych LANDSAT [Application of single-channel algorithm for mapping land surface temperature based on LANDSAT satellite data],* Roczniki Geomatyki 9, *4*, 139–149 (in Polish, summary in English).

Walawender, J.P., Hajto, M.J., and Iwaniuk, P. (2012), *A new ArcGIS toolset for automated mapping of land surface temperature with the use of LANDSAT satellite data,* Proc. IEEE IGARSS, 22–27 July 2012, Munich, Germany, 4371–4374, doi: 10.1109/IGARSS.2012.6350405

Walczewski, J., and Feleksy-Bielak, M. (1988), *Diurnal variation of characteristic sodar echoes and the diurnal change of atmospheric stability,* Atm. Environ. *22*, 1793–1800.

Weng, Q. (2001), *A remote sensing-GIS evaluation of urban expansion and its impact on surface temperature in the Zhujiang Delta, China,* Int. J. Remote Sens. *22*(10), 1999–2014.

Weng, Q. (2009), *Thermal infrared remote sensing for urban climate and environmental studies: Methods, applications, and trends,* ISPRS J. Photogramm. Remote Sens. *64*, 335–344.

Xiao, R., Ouyang, Z., Zheng, H., Li, W., Schienke, E. W., and Wang, X. (2007), *Spatial pattern of impervious surfaces and their impacts on land surface temperature in Beijing, China*, J. Env. Sciences *19*, 250–256.

Yilmaz, R. (2010), *Monitoring land use/land cover changes using CORINE land cover data: a case study of Silivri coastal zone in Metropolitan Istanbul*, Environ. Monit. Assess. *165*, 603–615.

(Received August 1, 2012, revised April 19, 2013, accepted May 14, 2013, Published online July 2, 2013)